Surv Geophys (2012) 33:1177–1230
DOI 10.1007/s10712-012-9196-9

Global Dynamics of the MLT

Anne K. Smith

Received: 14 February 2012 / Accepted: 10 May 2012 / Published online: 19 June 2012

Abstract The transition between the middle atmosphere and the thermosphere is known as the MLT region (for mesosphere and lower thermosphere). This area has some characteristics that set it apart from other regions of the atmosphere. Most notably, it is the altitude region with the lowest overall temperature and has the unique characteristic that the temperature is much lower in summer than in winter. The summer-to-winter-temperature gradient is the result of adiabatic cooling and warming associated with a vigorous circulation driven primarily by gravity waves. Tides and planetary waves also contribute to the circulation and to the large dynamical variability in the MLT. The past decade has seen much progress in describing and understanding the dynamics of the MLT and the interactions of dynamics with chemistry and radiation. This review describes recent observations and numerical modeling as they relate to understanding the dynamical processes that control the MLT and its variability. Results from the Whole Atmosphere Community Climate Model (WACCM), which is a comprehensive high-top general circulation model with interactive chemistry, are used to illustrate the dynamical processes. Selected observations from the Sounding the Atmosphere with Broadband Emission Radiometry (SABER) instrument are shown for comparison. WACCM simulations of MLT dynamics have some differences with observations. These differences and other questions and discrepancies described in recent papers point to a number of ongoing uncertainties about the MLT dynamical system.

Keywords Mesopause · Gravity waves · Tides · WACCM · SABER

1 Introduction

The region of transition from the middle atmosphere to the thermosphere is known as the MLT (mesosphere and lower thermosphere). This region exhibits a balance of processes not seen elsewhere in the atmosphere and is often treated as a separate region. Much has

A. K. Smith (✉)
NCAR, P.O. Box 3000, Boulder, CO 80307, USA
e-mail: aksmith@ucar.edu

been learned about the MLT in recent years through additional observations and improved numerical modeling capabilities. This survey will describe the dynamics of the MLT, with emphasis on recent developments and ongoing questions.

The concepts will be illustrated primarily with the results from simulations made with the Whole Atmosphere Community Climate Model (WACCM). WACCM is a component of the Community Earth System Model, a family of model components at the National Center for Atmospheric Research (NCAR). WACCM is a comprehensive global climate model that extends from the Earth's surface into the lower thermosphere. It includes interactive chemistry with realistic surface concentrations and trends of natural and anthropogenic trace gases. External forcing by solar variability and energetic particle fluxes is also included. Model results shown here are from extended integrations using WACCM version 3.5. This version does not include interactions between the atmosphere and the oceans; instead, sea surface temperatures are specified using observations from recent decades. Descriptions of the formulation of dynamics and the external forcing in WACCM version 3.5 are given by Garcia et al. (2007), Marsh et al. (2007), Richter et al. (2010), and Smith et al. (2011). Extensive comparisons of WACCM with other models are presented by Eyring et al. (2006) and WMO (2010). There is also an extended version of the model, WACCM-X, that has an upper boundary at 2.5×10^{-9} hPa ($\sim$500 km altitude) (Liu et al. 2010).

The topics covered in this paper are the characteristics of the large-scale winds and temperatures, the balances that maintain the basic state, the description of waves and their interactions, the dynamical coupling between the MLT and the rest of the middle atmosphere, and the response of the MLT dynamical environment to external forcing by anthropogenic composition changes and solar variability. Companion papers by Feofilov and Kutepov (2012) and Sinnhuber (2012) discuss the MLT radiative balance and the response of MLT chemistry to energetic particles, respectively. Although this paper gives many references for observational and theoretical studies, the reference list is not comprehensive. The topics discussed and the interpretation reflect the interests and experience of the author.

For other reviews of MLT dynamics, see Shepherd (2000), Becker (2011), and Smith (2011). Shepherd (2000) addresses the development of our understanding of some key phenomena in the stratosphere and mesosphere since the middle of the twentieth century. Becker (2011) focusses particularly on the mean circulation and the processes that control it. Smith (2011) reviews the processes involved in the interactions between the lower, middle, and upper atmosphere. A review of whole atmosphere models by Akmaev (2011) also discusses current understanding of the role of the MLT in coupling between atmospheric regions.

2 Measurements and Their Limitations

Measurements of the MLT dynamical conditions have been made remotely using ground- and space-based instrumentation and in situ using rockets. None of the instrumentation can give a complete picture, but together they provide a more rounded picture of the basic state and its variations than is possible with any single measurement technique. Ground-based and rocket-borne instruments have limited geographic extent but can provide high vertical resolution. Continuous ground-based observations give a great deal of information about local time variations. Satellite instruments provide a global or near-global picture but have limited local time sampling, and many also have limited spatial resolution. The primary

dynamical fields that can be determined from measurements are kinetic temperature, neutral density, vectors of horizontal winds, and small-scale perturbations to airglow emissions caused by waves. Specialized measurements such as turbulence have also been taken.

Passive ground-based observations use light emitted in the MLT to deduce properties of the atmosphere. The light sources used are various airglow emissions which, depending on the chemical processes that produce the light, come from different altitudes. OH Meinel emissions, which originate in a layer near 87 km, are used to deduce temperature and details of the evolution of small-scale waves. Other emissions used are the O_2 atmospheric band (91–95 km), the sodium D line ($\sim$90 km), and the oxygen green line (95–100 km). These measurements are limited to nighttime and sky conditions that are clear or have a light overcast. Visible observations of polar mesospheric clouds in high-latitude summer provide a limited duration but striking method of observing waves in the MLT.

Temperature (e.g., Taylor et al. 1999) and wave properties (e.g., Takahashi et al. 2002; Hecht 2004; Simkhada et al. 2009) can be determined from OH nightglow emissions. There is an element of uncertainty because the dynamical perturbations that change the temperature also affect the altitude of the emitting layer, which can move up or down by several kilometers due, for example, to displacement by tides. Long records of measurement of temperature from ground-based OH emissions (Bittner et al. 2002; French and Mulligan 2010; French and Klekociuk 2011) are useful in determining long-term trends (see Sect. 7) There has also been effort to use two or more different types of ground-based instruments at the same site for additional insight into the dynamics (Ejiri et al. 2009; Taori et al. 2011).

Active ground-based observations are made by radar and lidar. Two types of radar are commonly used for winds in the MLT. Meteor radars use the reflection of radio wave pulses by meteor trails (e.g., Mitchell et al. 2002), and medium frequency (MF) radars use reflections by changes in the refractive index in the clear atmosphere (e.g., Vincent et al. 1998). With two or more beams tilted from the vertical, radar signals can be processed to yield horizontal vector winds. Many radar stations operate unattended 24 h per day and are therefore able to give a continuous record that can be used to determine tides, gravity waves, and other high-frequency variations. Density variations detected by lidar can be used to determine temperature. Some lidars also measure horizontal winds (e.g., Baumgarten 2010). Early lidars operated only during night but, with improved technology, some instruments can operate during day as well (She et al. 2002). Their data coverage is less complete than for radar because no signal is obtained under cloudy conditions and also because the instruments are not fully automated. In a comparison of winds from co-located lidar and meteor radar, Franke et al. (2005) found good agreement; they concluded that most of the root-mean-square difference in the radar and lidar winds could be explained by the much higher vertical resolution of the lidar measurements.

Although the network of ground-based stations that observe mesospheric dynamical processes has increased, it is still not sufficient to provide a detailed global view. One major impediment to achieving this is that land covers less than half of the surface of the globe. In addition, some sites over land are not accessible to lidar or passive optical techniques because of persistent cloud cover. Construction of a regional or global climatology by combining data from different ground-based instruments also has to take into account the bias between instruments.

Probing the MLT region by rockets has been performed intermittently. These measurements are most valuable when made as part of organized campaigns with multiple measurements. Rocket soundings are the only technique for in situ sampling on the MLT.

Measurements from rockets have another advantage over other techniques that it is possible to achieve very high verticle resolution. As discussed by Lübken (1997), density fluctuation over distances of a few meters allows the determination of turbulent energy dissipation rates. Rockets have also been used in active experiments in which a plume of substance, such as a chemical that fluoresces or bits of reflecting material that leave a visible trail, is released and observed from the ground. Due to the expense, contributions to MLT observations from rocket-borne experiments have been a decreasing part of the available database in recent decades.

Satellite instrumentation for dynamical variables has improved as instrument design has evolved to take advantage of improving sensors and other technology. However, the high cost and long development time strongly limit the number of instruments in orbit. Passive satellite measurements of the MLT rely either on emissions from the radiatively active trace chemical species or on modifications to the light from the sun or other stars as it passes through the atmosphere. Infrared emissions from CO_2 are used to determine temperature. Information about temperature can also be deduced from polar mesospheric clouds (PMC) since these clouds only form when the temperature is extremely low. Airglow emissions provide additional information about temperature and also, through Doppler shift, about horizontal winds in the line of sight. Profiles extending over broad vertical depth provide information about dynamical coupling between atmospheric layers.

Limb scanning is used in many satellite observations because of the potential for good vertical resolution (a few km). Data sets that have provided important information about MLT dynamics come from the Solar Mesosphere Explorer (SME), the Upper Atmosphere Research Satellite (UARS; 1991–2005), the Thermosphere Ionosphere Mesosphere Energetics and Dynamics satellite (TIMED; 2002–ongoing), the Envisat satellite (2002–ongoing), and the Cryogenic Infrared Spectrometers and Telescopes for the Atmosphere (CRISTA; November 1994; August 1997) missions. A major gap in information about the dynamics of the MLT could be approaching since TIMED and Envisat are already beyond their original design lifetimes. Successors for these aging but highly successful satellites are not currently under construction.

3 Climatology

The term climatology refers to multiyear averages and their seasonal variations. The climatology is useful for predicting general conditions to be seen at a particular location and time of year.

A long-time and well-used reference for the climatology in the mesosphere is the MSIS (mass spectrometer incoherent scatter) empirical model (Hedin 1991). The most recent version is known as NRLMSIS-00 (Picone et al. 2002). Because additional new satellite observations have been accumulating at a rapid rate since this was released in 2000, the MSIS description does not capture many details about the MLT dynamics, composition, and variability. The empirical model used for NRLMSIS-00 includes parameters to represent the changes with season, solar cycle, and geomagnetic activity. The related Horizontal Wind Model (HWM07) gives horizontal wind climatological fields (Drob et al. 2008). The HWM07 includes seasonal and local time variations due to planetary waves and tides during solar quiet times. There is also an option (DWM07) (Emmert et al. 2008) for the upper thermosphere during solar active periods.

The MLT climatology has been evolving in part due to new observations but also because the climate is itself not fixed. The state of the MLT region exhibits year-to-year

variations and trends in response to changing external forcing and changing atmospheric composition. The most important sources of trends and interannual variability are due to the anthropogenic changes in atmospheric composition, changes in the energy input from above (ultraviolet radiation from the Sun and energetic particles from the outer parts of the Earth system), and changes in the wave forcing from below. These are discussed in Sect. 7.

The climatological state of the MLT cannot be completely characterized due to the relatively short duration of most measurement records and to the large variability. As of now, there is not enough information to determine definitively how much of the variability is internal and how much is externally forced. In general, the regions below (i.e., the troposphere and stratosphere) have a more important impact on the MLT than vice versa (e.g., Liu et al. 2009). MLT variations forced from below are often considered to be externally forced.

In the lower atmosphere and in much of the middle atmosphere, the basic dynamics varies more with latitude and altitude than with longitude. The latitude × pressure or latitude × altitude view is considered to be the background basic state. Despite some very large amplitude waves in the MLT, particularly diurnal tides, the 2-D view is nevertheless a useful framework to examine seasonal and interannual evolution of the MLT dynamics. This section describes the basic state averaged in longitude and in local time. The important wave processes are described in Sect. 4

3.1 Zonal Mean Temperature and Winds

The most striking feature of the MLT is the temperature structure during solstice seasons. The upper panels in Fig. 1 show the mean temperature for 60-day periods centered on January and July determined from the Sounding the Atmosphere by Broadband Emission Radiometery (SABER) instrument on the TIMED satellite. Averages are from version 1.07 observations made between January 2002 and December 2011. TIMED precesses with a period of about 120 days. With day and night measurement taken on each orbit, almost all local times are observed in about 60 days. The 60-day averaging minimizes the aliasing from tidal temperature variations. Pressure on a logarithmic scale is used as the vertical coordinate; the global mean geometric altitude is given on the right axis. See also Huang et al. (2006), Xu et al. (2007a, b) for climatological temperatures using earlier versions of the SABER data.

The simulated average January and July temperatures from the WACCM model are shown in the lower panels of Fig. 1. See Garcia et al. (2007) and Richter et al. (2010) for some discussions of the WACCM simulations. There are a number of differences between the model and the observed temperature. One obvious difference is the temperature at the mesopause. SABER observations indicate that there is a pole-to-pole extension of low temperature around 95–100 km that is seen at both solstice seasons. This low temperature has been seen in other observations as well (e.g., von Zahn et al. 1996).

The mesopause is defined as the coldest point in the vertical profile. In the winter hemisphere and in low latitudes during all seasons, the daily mean altitude of the mesopause is near 100 km (Fig. 1). However, in the summer high latitudes, the mesopause temperature is much lower, and its altitude is lower (von Zahn et al. 1996; Xu et al. 2007a). The global low temperature at 95–100 km is due to the radiative balance there. As elsewhere in the middle atmosphere, CO_2 radiative transfer cools the MLT (Fomichev 2009; Feofilov and Kutepov 2012). The primary energy for heating in the MLT is absorption of solar energy by O_2. The link between absorption of energy and heating is complex in the MLT due to the loss of energy due to airglow emissions (Mlynczak and

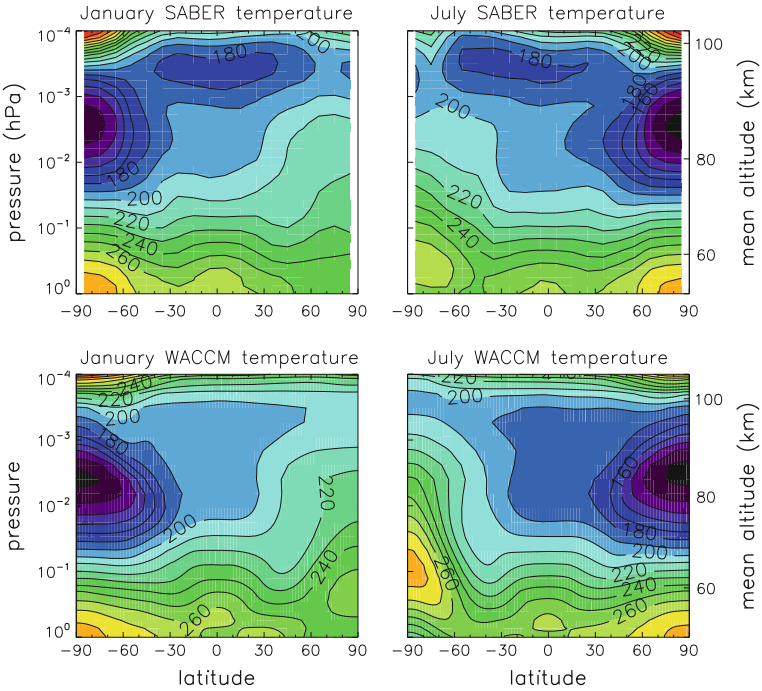

Fig. 1 *Top panels* are zonal mean temperature from SABER retrievals averaged over the years 2002–2011 for 62-day periods centered on January and July. *Bottom panels* are zonal mean temperature from WACCM averaged for a multiyear climatology 1960–2006 for January and July. Contour interval is 10 K

Solomon 1993) and the slow rate at which the energy of photolysis is eventually converted to heat. The low temperature is a result of the balance between the weak heating and the efficient radiation to space by CO_2. It is evident from Fig. 1 that the energy balance at 100 km simulated by WACCM has significant discrepancies from the SABER observations.

Another source of global heating and cooling is due to dissipating gravity waves and their interaction with the background atmosphere. See Sect. 4 for a brief discussion of the role of gravity wave heating. This contribution is very uncertain because of the lack of comprehensive observations. There are also different estimates of the net heating from different theoretical studies (e.g., Medvedev and Klaasen 2003; Becker 2004).

Leovy (1964) showed that the cold summer mesopause must be maintained by dynamical motion. The adiabatic cooling associated with strong rising motion is necessary to cool this region to temperatures well below the photochemical equilibrium conditions. Since the work of Lindzen (1981) and Holton (1983), the role of gravity wave propagation and dissipation has been accepted as the dominant wave forcing. Although new details have come to light with improved measurements, the basic explanation for the cold summer mesopause is still accepted. Recent developments have given a better description of the circulation with the help of numerical models (see Sect. 3.2) and have allowed a characterization of the differences between the two hemispheres (see Sect. 6.2)

Horizontal winds in the MLT are highly variable. Radar measurements show a very broad spectrum of variations from the annual timescale to short periods that are limited by the instrumental averaging time. Rapid movement of wave-like perturbations can be seen

in airglow images. Many of the observed variations are due to propagating waves. Sections 4.1 and 4.3 discuss two of the most important classes of waves: mesoscale gravity waves and tides. Averaging radar data over time, for example taking a monthly average, gives the time-mean wind and, using the assumption that the longitudinal variations of the time-mean fields are small, an estimate of the zonally averaged wind (Mitchell et al. 2002). Satellite observations (Smith 1997; Wang et al. 2000) show that there are planetary-scale variations in the monthly averaged horizontal winds in the MLT. Because of these persistent longitude variations, the time-mean wind at a radar site is likely to differ from the true zonal mean wind.

Multi-year observations from radar measurements in middle and high latitudes (e.g., Dowdy et al. 2007; Hoffmann et al. 2011) indicate that the summer zonal wind changes sign from easterly (from the east) to westerly around 90–95 km. The average winds during winter are westerly and do not change to easterly within the measurement range of the radars (up to 95–100 km). Although there are satellite observations of horizontal winds, some uncertainty remains because of the difficulty of determining the position on the detector that corresponds to zero wind (Burrage et al. 1993). More than a decade of satellite winds are available from the High-Resolution Doppler Imager (HRDI) on the Upper Atmosphere Research Satellite (UARS) and from the Wind Imaging Interferometer (WINDII) on the same satellite. McLandress et al. (1996) presented near-global MLT zonal winds from a combination of HRDI and WINDII data. The zonal wind climatology from WINDII has been updated by Zhang et al. (2007). Zonally averaged zonal and meridional winds from the TIDI instrument on the TIMED satellite have recently become available (Niciejewski et al. 2011).

The HRDI winds for the period 1991–1998 have been collected by the UARS Reference Atmosphere Project (URAP) and are combined with stratospheric winds from assimilation of meteorological data (Swinbank and Ortland 2003). The monthly URAP winds are available as a climatology. In middle latitudes during the solstice periods, the winds are easterly in the summer hemisphere and westerly in the winter hemisphere. Individual wind profiles can be quite variable and, during dynamically active periods, the entire structure can be changed in the winter hemisphere (see Sect. 5.1)

The URAP satellite winds shown in Fig. 2 are consistent with radar observations; both types of observations indicate that the winter wind reversal from westerly to easterly occurs at high altitude. In winter of both hemispheres, the reversal is at about 95 km (top panels of Fig. 2). Figure 2 also gives the average January and July zonal winds from WACCM. The seasonal pattern for the solstice periods (easterly in winter and westerly in summer) and the strengths of the jets are well represented in the model. Some aspects of the zonal mean winds simulated by WACCM differ from the observed winds. Although the radar winds at any given site could be affected by persistent longitudinal asymmetries (see Sect. 4.4), the radar wind measurements and the URAP climatological winds are consistent in showing westerly winds extending up to the mesopause. The much lower altitude for the winter transition from westerly to easterly wind in WACCM suggests that the discrepancy is likely a problem with the model simulation.

Lieberman et al. (1993) showed that the tropical winds measured by HRDI at 80 km have a strong semiannual oscillation (SAO) with peak easterly winds in the equinox seasons. The oscillation can also be seen in the URAP winds for the band 10°S–10°N (Fig. 3). The mesospheric SAO in WACCM, also shown in Fig. 3, has smaller magnitude than that observed. This oscillation is believed to be driven by gravity waves; see Sect. 4.1.3. The discrepancy may indicate a problem with the WACCM gravity wave forcing at this altitude region in the tropics. In addition, the tropical view in Fig. 3 indicates that

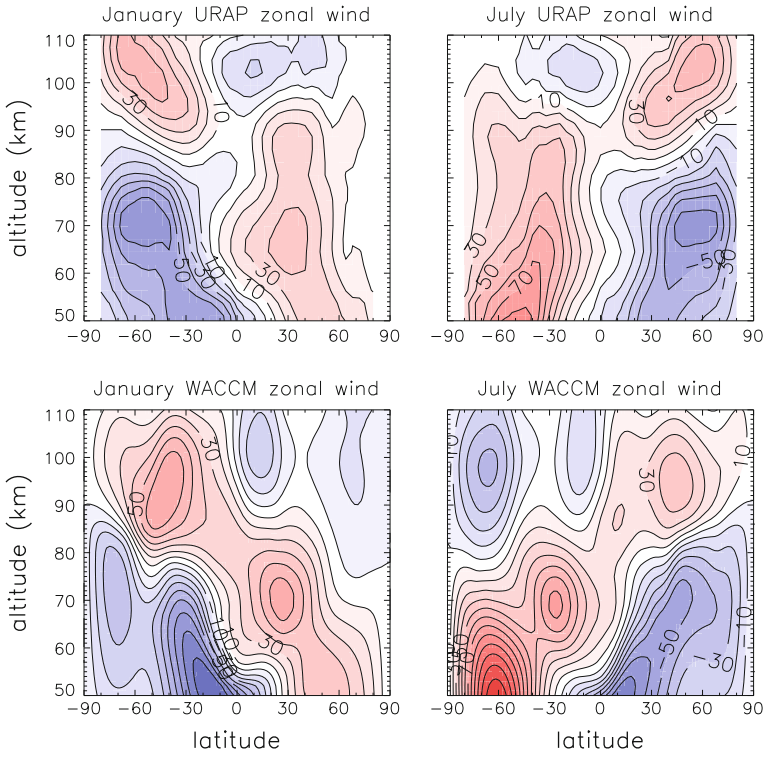

Fig. 2 Zonal mean zonal wind from the URAP climatology (*upper panels*; 1992–1995) and simulated by WACCM (*lower panels*; multiyear climatology 1960–2006) for January and July. Contour interval is 10 m/s

westerly winds prevail in the range 70–85 km, whereas the HRDI observations show predominantly easterly winds at these altitudes. The HRDI observations show that a small SAO is present as high as 100 km, whereas no comparable oscillation is simulated in WACCM.

Observations (e.g., Huang et al. 2006; Xu et al. 2007a) also indicate that there is an interannual variation in the zonally averaged temperature in the MLT that is related to the quasi-biennial oscillation (QBO) in tropical lower stratospheric winds and temperature. The driving mechanism for this may be the same as that for the SAO in the MLT, see Sect. 4.1.3. In a study using several decades of data, Ratnam et al. (2008) showed that the relationship between the stratospheric and mesospheric QBO in winds varies with time. However, some of the data they analyzed for this study have limited local time coverage so the analysis results could include aliasing from the diurnal tide, which itself has a substantial QBO variation in amplitude (see Sect. 4.3.1)

3.2 Mean Meridional Circulation

The temperature structure during solstice periods (Fig. 1) is consistent with net upwelling near the summer pole (adiabatic cooling is responsible for the low temperatures) and sinking near the winter pole. However, details of the circulation are difficult to measure directly. For this, we rely on numerical models that include the radiative forcing as well as

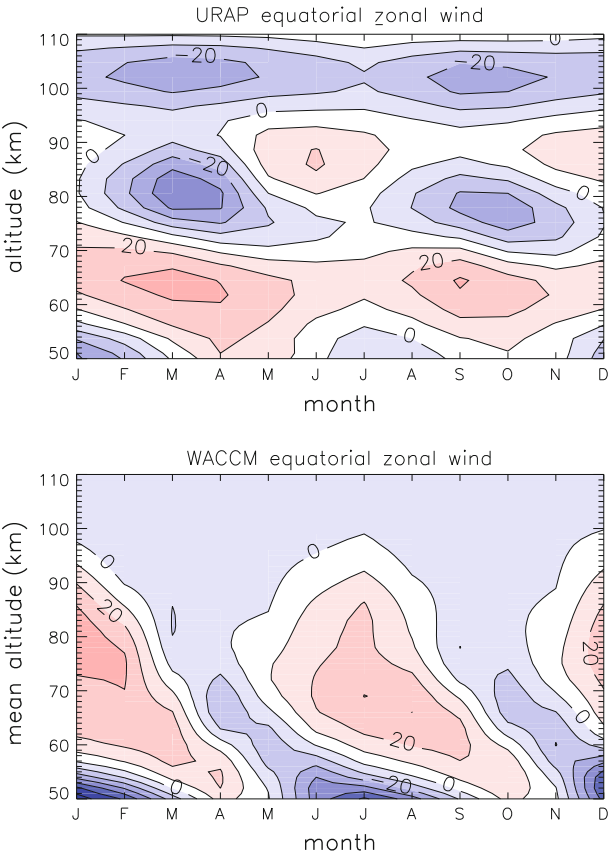

Fig. 3 Annual variation of monthly mean zonal wind from URAP (*upper panels*) and WACCM climatology (*lower panel*) averaged over the latitudes 10°S to 10°N. Contour interval is 10 m/s

the dynamical forcing. Throughout the middle atmosphere, the large-scale motion is driven by waves (Andrews et al. 1987).

In principle, the mean atmospheric circulation for monthly or longer time periods can be diagnosed from the diabatic heating (see discussion of the diabatic circulation by Dunkerton 1978). In practice, it is difficult to determine the diabatic heating because the concentrations of radiatively active gases are not well known due to high variability, including rapid diurnal changes, and also because radiative transfer is complex in the MLT because the CO_2 emissions responsible for most of the cooling are not in local thermodynamic equilibrium (LTE; see Feofilov and Kutepov 2012). Lieberman et al. (2000) derived the diabatic circulation using temperature measurements from HRDI. The calculated meridional winds did not show consistent agreement with either the meridional winds measured by HRDI or with time average winds measured by radar at several latitudes.

The net air motion associated with the circulation is best viewed in the transformed Eulerian mean system proposed by Andrews and McIntyre (1976). This transformation defines new meridional and vertical mean velocities, denoted $\overline{v}^*$ and $\overline{w}^*$, that better represent the actual motion of air parcels. $\overline{v}^*$ and $\overline{w}^*$ are also known as the residual velocities. In the MLT, the transformed Eulerian velocities are similar to the conventional Eulerian mean velocities because planetary waves are not a dominant part of the wave field.

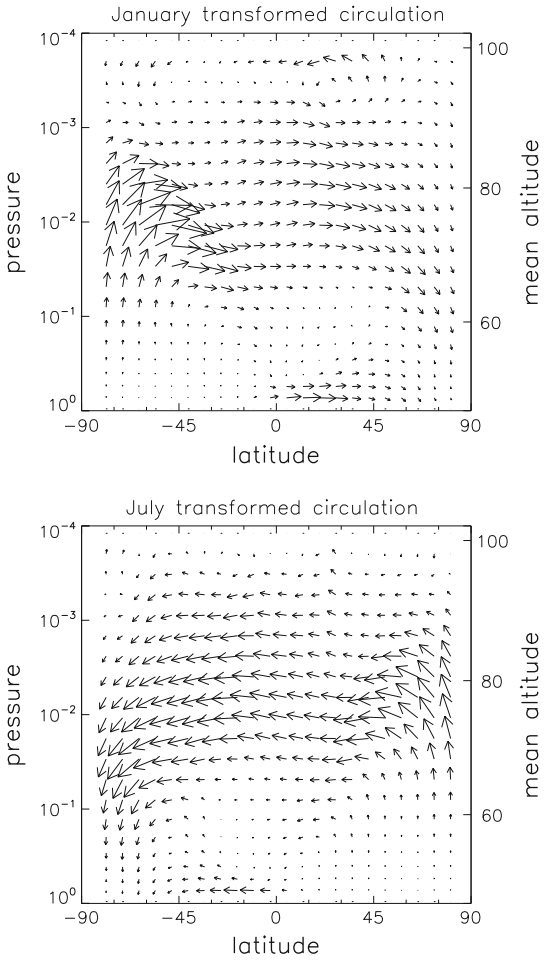

Fig. 4 *Arrows* showing the direction of the transformed Eulerian mean meridional circulation from a multiyear climatology simulated by WACCM. *Top* is the average for January; *bottom* is the average for July

Figure 4 gives the average WACCM mean circulation in vector form for the months shown in Fig. 1. The derivation of the circulation in WACCM is described by Smith et al. (2011). Figure 5 shows the magnitudes of the meridional and vertical components of the circulation during January and July. The zonal momentum forcing due to gravity waves in WACCM is shown in Fig. 6.

There are indirect ways of verifying that the basic circulation estimated from theory and numerical models is reasonable. First and foremost is the simulation of the temperature structure, particularly the horizontal structure such as the cold summer and warm winter mesopause. As seen by comparing WACCM temperatures with SABER observations (Fig. 1), the qualitative agreement in temperature is good. For example, in both cases, the summer minimum temperatures in both hemispheres are 120–130 K. This implies that the transformed Eulerian mean circulation simulated in WACCM (Fig. 4) is realistic. However, the altitudes of the summer temperature minima are slightly lower in WACCM than in the SABER observations. Another discrepancy is the penetration of warm air to higher altitude in the SH winter (June–July) in WACCM. Since the transformed Eulerian mean circulation is a wave-driven flow, the discrepancies imply that the magnitude or vertical

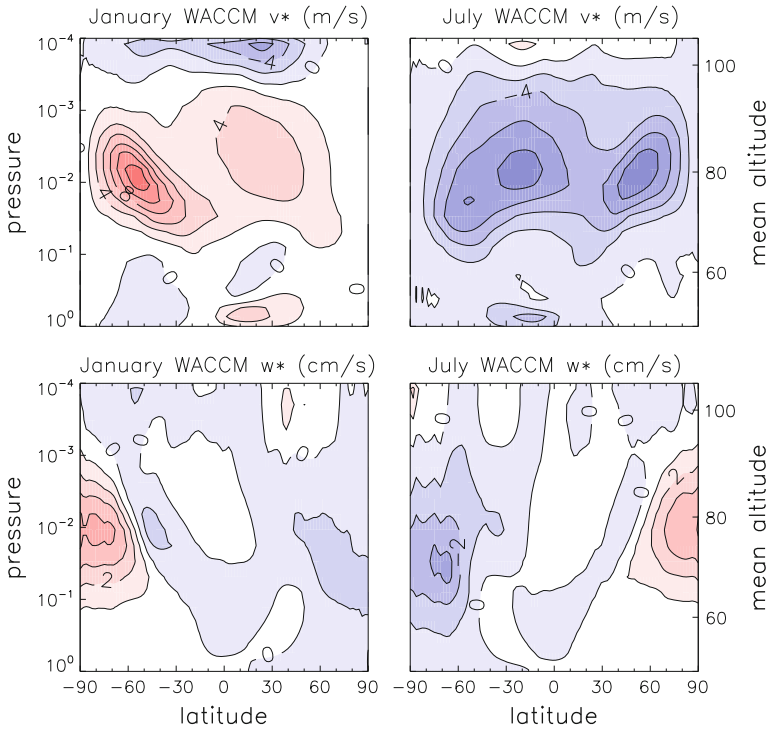

Fig. 5 The meridional and vertical components of the transformed Eulerian mean meridional circulation from a multiyear climatology simulated by WACCM for January (*left*) and July (*right*). Contour interval is 2 m/s for the meridional component and 1 cm/s for the vertical component

distribution of the wave momentum or energy deposition in WACCM is not completely accurate. The dominant wave process causing the low temperatures in the summer mesopause is forcing by gravity wave dissipation and breaking, which is parameterized in WACCM. Comparisons of the global mean temperatures suggest that the heating due to gravity wave processes may contribute to the discrepancy between the model and the SABER-observed temperature.

Additional validation of the strength and direction of the circulation comes from the simulation of trace species that are affected by transport. As shown by Smith et al. (2011), comparison of the WACCM simulation of the distributions of water and atomic oxygen with observations suggests that the poleward branch of the circulation in NH winter occurs at an altitude that is too low by a few kilometers. Since the circulation is driven primarily by momentum forcing introduced into the model by the gravity wave parameterization, this suggests that the parameterization needs to be modified. There are several parameters that are poorly constrained by observations. These were adjusted to give a good overall representation of the winds and temperature in the entire middle atmosphere. Since each single parameter affects the simulation in all seasons, latitudes and over a broad vertical range, perfect agreement of the simulations with observations is not feasible. Gravity wave parameterizations in numerical models are discussed further in Sect. 4.1

For direct comparison of WACCM simulations with observations in the past decade, the model is run in specified dynamics mode, known as SD-WACCM. In this mode, key tropospheric and stratospheric dynamical variables are constrained by meteorological

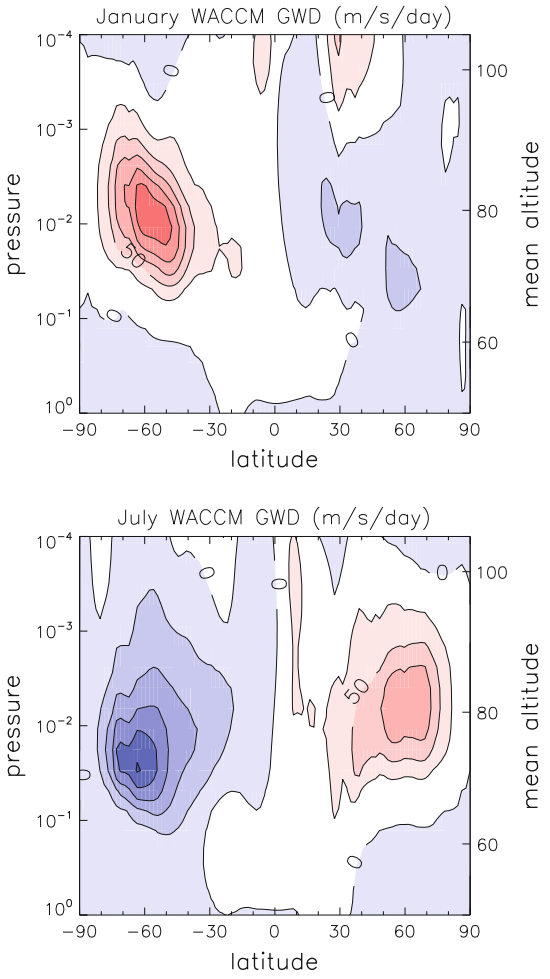

Fig. 6 Zonal component of gravity wave forcing from WACCM averaged for a multiyear climatology 1960–2006. *Top* is the average for January; *bottom* is the average for July. Contour interval is 25 m/s/day

analyses from weather prediction models that assimilate observations. Marsh (2011) used this version of the model to examine dynamical and chemical evolution during the 2005–2006 NH winter. He found that the evolution of events during this highly active period (see Sect. 5.1) closely followed the observations, even in the upper levels where no constraints were placed on the model. This gives support for the model dynamics in the mesosphere and for the reliability of the mean circulation derived from WACCM. Additional evidence comes from model experiments to investigate chaotic growth of errors using WACCM. Liu et al. (2009) showed that the error growth in the MLT is much reduced when the lower atmosphere is constrained by reinitializing daily.

4 Waves

In general, the term wave is used for a disturbance that propagates in space and time. Three features of waves are important: generation, propagation, and dissipation. The generation will receive less attention in this paper because the bulk of the wave activity in the MLT

originates below, in the troposphere or stratosphere. However, secondary waves that are created by the interactions of waves can be generated anywhere in the system, including in the MLT.

Waves will not interact with the background atmosphere unless they are transient or dissipating. This noninteraction theorem, described by Andrews and McIntyre (1976), applies to Rossby waves, gravity waves, and tides. For all of these waves, the propagation conditions depend on characteristics of the wave and also on the background through which the wave propagates. The background zonal wind is particularly important because of its high speed and large seasonal (Fig. 2) and year-to-year variations.

Another concept that is useful for understanding wave behavior is that of critical layer (also called critical level). This is a point in the atmosphere where the phase speed of a wave is equal to the speed of the background wind. Waves cannot propagate through this region; they will be dissipated or, in some circumstances, reflected. The critical layer concept is most useful for predicting the propagation of gravity waves and planetary waves because they have phase speeds whose magnitudes are within the range of middle atmosphere zonal and meridional winds.

4.1 Gravity Waves and Their Forcing of the Background Atmosphere

Although gravity waves are interesting in their own right and have been much studied, the focus of this section is on the impact of gravity waves on the large-scale dynamics of the MLT. For more about the gravity waves themselves, see the review by Fritts and Alexander (2003).

It is now widely accepted that gravity waves provide the bulk of the momentum forcing that drives the circulation in the MLT. This circulation is responsible for the cold summer mesopause and for much of the vertical transport of trace species (Sect. 3.2). This is not a one-way interaction. The generation, propagation, and dissipation of gravity waves depend on the winds and thermal structure of the surrounding environment. Gravity waves present a particular challenge for observations and numerical modeling because the scale of individual waves can be small (tens of km), whereas their cumulative impact is global.

Observations of gravity wave winds and/or temperatures are made by radars, lidars, and airglow imagers. The wave periods that can be seen are constrained on the short end by the time needed to make a measurement and on the long end by the instrument operation and the need to separate the waves from other atmospheric variation. Deducing some aspects of gravity wave structure (for example horizontal wavelength) from ground-based radar or lidar observations relies on theoretical relations such as the dispersion relation. The analysis can be enhanced by simultaneous observations of several coherent wave variables. Lidars that are capable of both wind and temperature data is one tool for this; another is the combination of simultaneous measurements from co-located ground-based instruments. Another type of observation that is especially useful for detecting waves with short wavelengths and periods is airglow imaging (e.g., Taylor et al. 1997; Snively et al. 2010).

Temperature profiles from limb-viewing satellites such as SABER also contain signatures of gravity waves. The gravity waves that can be detected are limited by the inherent spatial averaging of limb viewing and the vertical resolution (Alexander and Barnet 2007). However, if these limitations are properly treated in the analysis, much can be learned about gravity waves due to the near-global coverage of satellite observations. Preusse et al. (2009) calculated temperature variance from SABER data as an indictor of gravity wave activity. Another approach for determining gravity waves from satellite data was used by

Chandran et al. (2010). They reported on the horizontal structure of gravity waves derived from satellite images of polar mesospheric clouds.

Despite the improvements in techniques and the accumulating database of gravity wave measurements, the incomplete availability of measurements is one of the main limitations in characterizing the dynamical system in the MLT. This is further complicated because, due to limitations in computing resources, full interactive general circulation models do not currently perform integrations with sufficient resolution to simulate the generation, propagation, and dissipation of the small-scale waves.

4.1.1 Gravity Wave Sources and Conditions for Vertical Propagation

Ideally, observations could be used to follow individual waves from their point of origin in the troposphere to the region where they dissipate in the mesosphere. However, this is not normally practical for several reasons. (1) The amplitudes of gravity waves that are not dissipating grow approximately exponentially with altitude. Waves that are seen in the MLT have very small amplitudes in the troposphere. (2) Individual measuring systems do not cover the entire vertical range. (3) Gravity waves propagate horizontally as well as vertically so they may move beyond the ranges of instrumentation at a fixed location. Despite these limitations, there has been progress in linking gravity waves in the MLT with their sources below.

Sato et al. (2009) used simulations with a high-resolution global model that resolves gravity waves to look at the momentum fluxes in the middle atmosphere. Based on their analysis, they found several preferred regions for gravity wave sources. The locations of these regions are determined by two factors: tropospheric activity that generates the waves (by shear instability, flow over topography, or convection) and wind conditions that affect the ability for the waves to propagate vertically through the middle atmosphere. In the subtropics during summer, convectively forced gravity waves originating in the monsoon regions were important because these waves were able to propagate through the easterly winds in the stratosphere. In winter, gravity waves originated in the middle and high latitudes and propagated vertically and horizontally into the mesospheric jet regions.

Another approach for determining the gravity waves that affect the MLT circulation was taken by Preusse et al. (2009). They used temperature variance observed by SABER to estimate the gravity wave activity in the middle atmosphere. They also used a gravity wave ray tracing model to estimate where gravity waves launched from various spots on the globe would propagate. The ray-tracing approach included the refraction of the waves in the horizontal direction. The refraction depends strongly on the winds in the middle atmosphere and on properties of the gravity waves themselves, for example, horizontal wavelength, phase speed, amplitude. In the Preusse et al. (2009) study, the gravity wave sources were homogeneous and isotropic but, at each launch site, included waves with different characteristics. The results showed a good comparison of the simulations with the observed gravity wave variance. One finding of this study is the importance of latitudinal refraction of gravity waves. In this regard, the Preusse et al. (2009) study supports the finding from the Sato et al. (2009) study. Both studies indicate that horizontal as well as vertical propagation of the gravity waves that drive the MLT circulation should be taken into account. Additional observational evidence for the importance of horizontal propagation was found by Ern et al. (2011). Using the analysis of observations from SABER along with high-resolution observations from the lower and middle stratosphere, they found that the momentum flux from gravity waves generated in the tropical region affected the winds in midlatitudes.

4.1.2 Gravity Wave Processes in Global Models

The challenge of simulating gravity wave impacts in global models stems from the small horizontal scales of the waves compared to the typical grid of a global numerical model and from the deep vertical domain extending from the Earth's surface to the MLT. Even if the gravity waves themselves can be resolved, the complex dynamics during the wave breakdown requires even finer spatial and temporal resolution. However, proper simulation of the impacts of gravity waves, either through resolving the waves and their interactions with the larger scale or through parameterization, is necessary for all models of the global MLT.

There has been progress in modeling in which the waves themselves are resolved. In the spectral general circulation model (GCM) discussed by Watanabe et al. (2008) and Sato et al. (2009), gravity waves are generated self-consistently by topography at the surface or by dynamical processes in the troposphere. The waves propagate laterally as well as in the vertical direction. The model simulations are useful for investigating the generation of gravity waves and their propagation to the point where they break or dissipate and interact with the background atmosphere. The model top is near 85 km, so it stops short of simulating the full MLT region.

Another global model that resolves gravity waves was described by Becker (2009). This model is primarily focused on gravity waves and simplifies other atmospheric processes. For example, the radiative forcing to the atmosphere is approximated as a linear damping, convection is neglected, and the calendar is held fixed at January. Analysis of the model results shows that warming of the troposphere from anthropogenic climate change leads to a response in the MLT driven by gravity wave processes.

As noted, even a very high-resolution GCM cannot explicitly model the turbulence associated with breaking gravity waves. Some form of diffusivity is necessary to complete the interaction with the background flow when the scale of the perturbation fields of the wave is too small to be resolved by the model. The GCM described by Watanabe et al. (2008) and Sato et al. (2009) uses a Richardson number-based vertical diffusion to account for unresolved dynamical processes. It also includes a horizontal hyper-diffusion that is tuned to give a realistic spectrum of the waves. The Becker (2009) model also includes vertical and horizontal diffusion that plays a role in the interaction of gravity waves with the larger scales. In this model, both diffusivity parameters depend on the Richardson number.

Most global models with resolution too coarse to resolve the important gravity waves account for these processes by a parameterization. Holton (1983) gives an introduction to gravity wave parameterizations, and McLandress and Scinocca (2005) compare some of the parameterizations used in current models. The parameterization used in WACCM is based on the formulation by Lindzen (1981) with several updates (Richter et al. 2010) and uses a discrete spectrum of gravity waves. Figure 6 shows the climatological net zonal momentum forcing. Another parameterization used in several high-top models [the Canadian Middle Atmosphere Model (CMAM; McLandress and Scinocca 2005), the Hamburg Model of the Middle Atmosphere (HAMMONIA; Schmidt et al. 2006), and the Whole Atmosphere Model (WAM; Akmaev 2001b)] is based on work by Hines (1997a, b). Other gravity wave parameterizations have been proposed by Alexander and Dunkerton (1999), Medvedev and Klaasen (2000), and Warner and McIntyre (2001). Kim et al. (2003) discuss the assumptions about gravity wave spectra that go into the various parameterizations schemes.

All of the current gravity wave drag parameterizations are one dimensional (solved for a vertical column only) and include the following: a gravity wave source, a provision for the gravity wave to evolve and/or disappear based on the background through which it propagates, and a provision for the wave to exchange momentum with the background through dissipation and breaking. In the absence of damping, the gravity wave amplitude will grow approximately exponentially with height. Eventually, the amplitude is so large that the net temperature gradient (wave plus background atmosphere) is convectively unstable, and the wave will break. Parameterizations include a discrete or continuous spectrum of gravity wave phase speeds that extend into fast eastward and westward speeds (magnitudes $\geq$50–80 m/s). Topographically forced gravity waves with zero phase speed are often included as well; these can be important in the troposphere and stratosphere and sometimes penetrate to the mesosphere (Smith et al. 2009b).

In the earliest parameterizations, the tropospheric sources of gravity waves were a spectrum of zonally propagating gravity waves that were uniform at every point on the globe or were a uniform spectrum modified by the winds at the point where the waves were launched. An intermittency factor was needed, specifying that the waves were present for some fraction of the total time. Later, the sources and propagation were modified to take into account the 2-dimensional (meridional as well as zonal) background winds. A more recent development is for gravity wave sources that depend on the model dynamics. For example, in WACCM (Richter et al. 2010), gravity waves are launched when the conditions indicate the presence of fronts or convective activity. The convective source is most important in the tropics although it also plays a role in the summer over land surfaces. The frontal source is most important in middle and high latitudes. With the interactive sources, a specified intermittency factor is no longer needed.

The impact of the background on gravity wave propagation is the single largest factor affecting the seasonal cycle in dynamics in the MLT. As shown in the first global model with a gravity wave parameterization (Holton 1983), the first-order impact is the filtering of gravity waves in the stratosphere by critical layer processes. Investigation by McLandress and Scinocca (2005) indicates that this is still the most important component to the more sophisticated parameterizations currently in use. Waves with a particular phase speed will not be able to propagate vertically through a layer where the wind speed is equal to the wave phase speed. This filtering process explains the momentum fluxes of waves that reach the MLT. The breaking or dissipation of those waves leads to the reversal of the winds from the stratosphere to the mesosphere during the solstice seasons.

The final element in a parameterization is a representation of the impact of a breaking or dissipating gravity wave on the background atmosphere. In all parameterizations, this includes an exchange of momentum between the wave and the background. It is this momentum exchange that drives the winter westerly and summer easterly winds in the MLT.

Gravity wave parameterizations differ in the specification of the wave behavior and in the wave impacts on temperature and the distribution of trace chemical species. One difference is the fate of a wave that reaches breaking amplitude. That could result in damping of the wave to stay at an amplitude that is just below the breaking amplitude; this assumption was used in the formulation of Lindzen (1981) and Holton (1983) and is used in WACCM (Garcia et al. 2007). Another assumption that the wave disappears completely after it breaks was proposed by Alexander and Dunkerton (1999).

The thermal impact of gravity wave dissipation is another process that is treated differently in different gravity wave parameterizations. The potential thermal impacts are convergence of heat flux by the wave, diffusion of heat by turbulence, and heating due to

the conversion of kinetic energy to heat. A mix of positive and negative values (heating and cooling) was estimated by Liu (2000) and shown in modeling by Becker and McLandress (2009). Since the radiative heating is relatively weak in the MLT (this weakness is the reason for the very low temperatures there), gravity wave processes can make a substantial contribution to the global mean heating/cooling.

4.1.3 Impact of Gravity Waves on the MLT

The zonal winds in the MLT at middle and high latitudes change in response to interaction with breaking or dissipation of gravity waves. As noted above, the filtering of the gravity wave spectrum by the large background zonal winds in the stratosphere during solstice seasons is the key process that is responsible for the direction of the mesospheric zonal winds. There is evidence that the filtering of gravity waves accounts for other MLT variations as well.

The SAO in tropical upper mesospheric winds (Lieberman et al. 1993; Garcia et al. 1997) is out of phase with the SAO in the upper stratospheric winds. Dunkerton (1982) showed in a simple model that filtering of gravity waves by the stratospheric SAO affects the phase-speed distribution of gravity waves that penetrate to the mesosphere. When these waves break, they drive the mesospheric SAO. This was examined further by Sassi and Garcia (1997) and Ricciardulli and Garcia (2000). They found that dissipation of convectively forced waves by the SAO in the tropical stratosphere could account for the large SAO in the MLT.

Gravity waves can respond to or affect other waves through the sources, the propagation, or the interaction at dissipation. Smith (2003) showed that stationary planetary wave structures in the zonal wind in the MLT were out of phase with those in the stratosphere. The MLT planetary waves had two possible sources: they could propagate up from the stratosphere with a longitude shift due to the vertical wavelength of propagating Rossby waves, or they could be forced in situ by the dissipation of gravity waves that had been filtered by winds in the stratosphere. Numerical simulations indicated that both these processes were occurring.

It has long been known from radar observations that gravity waves vary depending on the phase of the diurnal (24 h) tide. This is primarily due to the same filtering process that affects gravity wave response to mean winds. The impact of gravity waves on the migrating diurnal tide is larger than for other migrating tides because the tidal vertical wavelength is shorter. A shorter vertical wavelength is associated with stronger wind shears and temperature gradients from the tidal perturbations, and so it can have an impact on gravity wave propagation. The gravity wave interaction with tides is noteworthy because the gravity waves can affect the downward propagation of tidal perturbations, thereby altering the wavelength of the tide. Ortland and Alexander (2006) used a model calculation to demonstrate how gravity waves can change the vertical wavelength of the DW1 tide. Watanabe and Miyahara (2009) found a similar impact of gravity waves on the tidal vertical wavelength in a gravity wave-resolving GCM.

Gravity wave interactions can also damp or amplify the tides when the gravity wave breaking occurs during different phases of the tide. Analysis of TIMED observations by Xu et al. (2009a) showed that the impact of unresolved processes (presumed to be gravity waves) is primarily to damp the diurnal migrating tide. Using the same data, Lieberman et al. (2010) found that the most important effect was to shorten the vertical wavelength of the tide.

4.2 Diffusion

Although it is acknowledged that diffusion can be important in the MLT, there is not a consensus about the magnitude or distribution of diffusion. One source of the problem is that the term diffusion is used to indicate several different processes.

Molecular diffusion is the name given for the dispersal and mixing of gases due to long pathlengths at the low density of the upper atmosphere. The impact of molecular diffusion increases as the density of the surrounding gas decreases. Molecular diffusion is further affected by molecular mass since the impact of gravity becomes competitive at the low collision rates. As the dispersive tendency based on mass becomes more important in the thermosphere, the dominant gases separate. The result is that lighter gases overlie heavier ones. The term molecular diffusion is used both for the mixing process and for the dispersive effect.

Models and observations indicate that molecular diffusion affects the composition of some gases in the MLT such as CO_2 (López Puertas et al. 2000; Beagley et al. 2010) and atomic oxygen (Smith et al. 2011). Molecular diffusion can have a direct effect on the dynamics through the transport of heat. The exchange of molecules from higher levels due to the long mean free path can lead to heat exchange. Transport of atomic oxygen, which releases heat when it is involved in any of several exothermic reactions (see Mlynczak and Solomon 1993), also is an effective means of transporting heat vertically in the MLT.

The term eddy diffusion is used for two different processes; they are likely related although the nature of the relationship is not clear. On the one hand, eddy diffusion indicates turbulent diffusion such as that responsible for the meteor trail dispersion observed by Kelley et al. (2003) or from the trails of chemicals released from a rocket (Bishop et al. 2004). Turbulence measurements have also been made by incoherent scatter radar (Hall and Hoppe 1998). At present, these measurements are not used in global-scale analysis or model evaluation. To do so would require an understanding of how processes on very small spatial scales and short duration are related to large-scale processes. One path for addressing the link may be the use of turbulence models within larger scale simulations. Liu et al. (1999) used a turbulence model along with a gravity wave model in a mesoscale simulation to investigate the transport effects of a breaking gravity wave. They found that the turbulence affected not only the rate of transport but also the propagation of the gravity wave. Areas of turbulence were not uniformly distributed along the wavelength of the wave. The resulting implied eddy diffusion coefficient, based on induced changes to trace gases, was less than that determined from the gravity wave saturation in the Lindzen (1981) formulation.

The term eddy diffusion is also used to include all unresolved processes that mix heat or chemical constituents; see Garcia et al. (2007) for a derivation showing how the heat flux convergence by a dissipating gravity wave can be represented as a vertical diffusion. Gravity waves that are dissipating give a net heat flux convergence that can be positive (heating) or negative (cooling). However, Akmaev (2007) argued that it is not completely accurate to represent the net heat flux convergence by gravity waves with a diffusion coefficient.

A parameter that is used in the diffusion coefficients from gravity wave parameterizations is the equivalent Prandtl number, Pr. The equivalent Prandl number represents the ratio of momentum flux to heat flux. It can be visualized in terms of the local nature of wave breaking (Coy and Fritts 1988). When breaking conditions are found over part of the wave, instead of along its full horizontal wavelength, Pr is greater than 1. A larger equivalent Prandl number means a lower rate of eddy diffusion applied to heat and trace

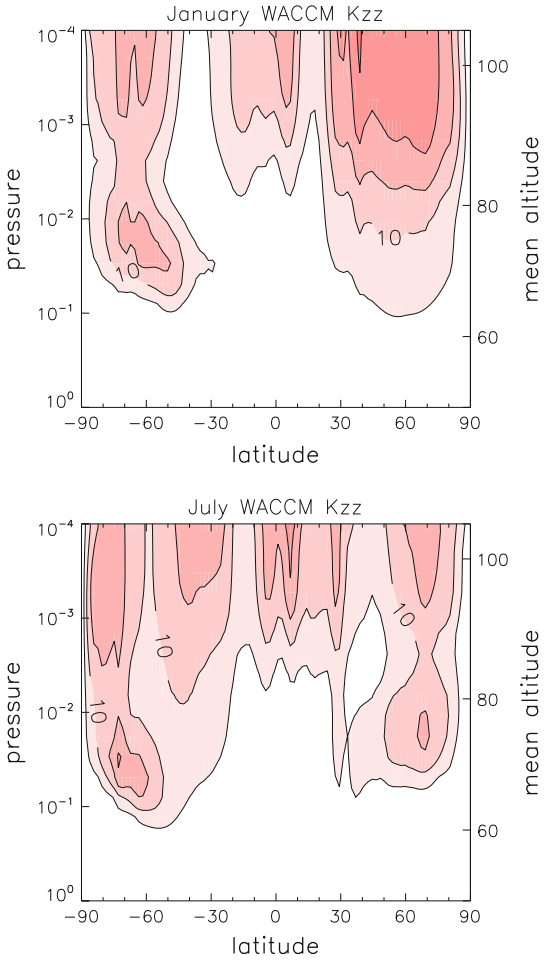

Fig. 7 Eddy diffusion rate from WACCM multiyear climatology for January and July. Contour interval is 5 m^2/s

species. The value adapted in models is normally in the range of 3–5. WACCM, for example, uses $Pr = 4$.

Liu (2009) determined the thermal eddy diffusion coefficient from lidar observations of resolved gravity waves. He found diffusion coefficients that varied with season in the range of 100–1,000 m^2/s. Grygalashvyly et al. (2011) calculated the effective diffusivity due to gravity waves from a gravity wave-resolving model. The derived effective diffusion coefficient was different for different trace species but, for the species they show, reached magnitudes of several hundred m^2/s. Figure 7 shows the climatological eddy diffusion rate from WACCM for January and July. These values are much smaller than the eddy diffusion estimated by Liu (2009) and Grygalashvyly et al. (2011). These and other large discrepancies between different estimates of diffusion are still not resolved.

The term "turbopause" refers to the altitude where turbulent motion ceases. Conventionally, it has been considered the altitude where the molecular diffusion coefficient becomes as large as the eddy diffusion coefficient. A related concept, the homopause, refers to the altitude where long-lived gases are no longer well-mixed. Since the molecular

diffusion coefficient varies depending on the mass of the chemical species in question, it is now recognized that there is no single homopause.

Offermann et al. (2007) used standard deviations of temperature as a function of altitude in global data to identify a transition they labeled the wave turbopause. The concept behind their analysis is that, in the middle atmosphere where waves are damped by turbulent processes, the variance will not grow with height at the rate for a conserved wave of $\exp(z/2H)$, where z is altitude and H is scale height. However, when the damping ceases at the turbopause, the variance can grow much more rapidly. Using this transition as a signature of the wave turbopause, Offermann et al. (2007) found a clearly defined wave turbopause that varied with latitude and season over the range from about 80 to 100 km.

4.3 Tides

Tides continue to be a major focus of research, not just because of their large amplitudes but also because tidal modes and their variability are still not completely understood. The persistence of questions is in a way curious because the basic processes that account for tides have been long known. The theory for tides forced by solar heating in an isothermal atmosphere at rest and with no damping was well explained by Chapman and Lindzen (1970). This is known as classical tidal theory, and the tides that it predicts are known as classical tides. Although the classical conditions of isothermal and windless are never met in the global atmosphere, the observed tides bear a good resemblance to the classical predictions. However, surprising new things about tides are still coming to light. One new aspect is the recent awareness of the importance of nonmigrating tides (defined below). Another is the teleconnection involved in the global coupling. An ongoing puzzle is that there is no consensus explanation for the large seasonal variability of the migrating diurnal tide.

Atmospheric tides are gravity wave modes whose period is exactly one day or an integral fraction of a day. Most of the tides seen in the MLT region have propagated from below although they can be modified by local conditions. The tidal response to in situ forcing in the MLT by diurnal variations in the heating is very small compared to the tides that propagate from below (Smith et al. 2003).

Tides can lead to very large variations in winds, temperature, density, and many other atmospheric parameters (airglow emissions, densities of trace species, etc.). A major source of tides is the diurnal variation in heating. The heating in the troposphere comes from absorption of sunlight by water vapor and from latent heat release. Heating in the stratosphere is mainly by absorption of ultraviolet radiation by stratospheric ozone.

Before the 1990s, much of the information about tides in the MLT came from radar observations. These are still an important source of information because radars can detect the diurnal cycle of winds at a single geographic location. With data from a single radar, it is not possible to determine the global structure of the observed tides. However, data from simultaneous operation of multiple radars provide some information about latitudinal (Pancheva et al. 2002) or longitudinal (Murphy et al. 2006) variations. With data from precessing satellites such as UARS and TIMED, the global structure of the temperature and horizontal wind variations are now known. Unfortunately, these slowly precessing satellites cannot resolve short-term variations in the tides, which leaves a gap in the present knowledge. Another limitation to relying on satellite data to determine tides is that some tidal modes are aliased in data from polar-orbiting satellites (Oberheide et al. 2003).

Hough functions provide a set of orthogonal global solutions of the classical tidal equation. A given tidal frequency and wavenumber, for example a westward propagating

diurnal tide with wavenumber one, will project on to a set of Hough functions. The set of functions for any wavenumber and frequency combination includes symmetric (with respect to the equator) and asymmetric modes. The heating that forces the tide can also be projected onto Hough functions and varies with season as the heating evolves. The largest seasonal difference is between equinox seasons (heating roughly symmetric across the equator) and solstice seasons (maximum heating shifted to the summer hemisphere). In the classical tide case, the Hough mode projections of the heating determine the tidal response. Specifically, the Hough mode projection of the tides follows the Hough mode projection of the heating and is the same at all vertical levels. However, under realistic conditions, the Hough mode projection of the tides varies with altitude in response to damping and to interactions with the background atmosphere or other waves. A mathematical representation of the variations in tidal projections with altitude is the concept of generalized Hough modes (Ortland 2005a, b).

A technique to extract additional information about tides from limited observations using theory together with wind observations was described by Svoboda et al. (2005) and also used by Oberheide and Forbes (2008). They use Hough mode extensions (HMEs), a technique developed by Forbes and Hagan (1982), to create complete global tidal fields of zonal and meridional winds, vertical wind, temperature and density in the mesopause region from the limited amount of horizontal wind data from UARS.

It is useful to distinguish between migrating and nonmigrating tides. Migrating tides follow the motion of the Sun: for example, a wavenumber 1 westward propagation 24-h tide, a wavenumber 2 westward propagation 12-h tide, and so on. All other tides are called nonmigrating. They can be westward or eastward propagating or stationary. A common abbreviation system refers to the tides by a string of three symbols. The first indicates the period: D (diurnal) or S (semidiurnal); the second indicates the direction of phase propagation: E (eastward), W (westward), or S (stationary); and the third is an integer giving the zonal wavenumber. The classical tides are migrating: DW1, SW2, etc. Analysis of global observations from precessing satellites has shown that nonmigrating tides contribute a significant, sometimes dominant, amount to the total tidal amplitude or variability.

Diurnal variations in dynamical fields that are locally forced but do not propagate vertically are referred to as trapped modes. It is not always possible to determine, from observations, whether a disturbance is or is not propagating. Even when a distinction is possible, the nomenclature can be imprecise. An example is the daily temperature perturbations in the stratosphere due to ozone heating. The temperature fluctuations are normally separated into frequencies that are subharmonics of 24-h (diurnal, semidiurnal, etc.) and considered to be tides. Some fraction of these temperature fluctuations maps onto Hough modes that can propagate vertically while quite a bit of the diurnal signal does not. The Hough modes that do not propagate are also called tides and are referred to as trapped modes.

4.3.1 Migrating Diurnal Tide

The best-studied tide is the migrating diurnal tide, DW1. There are a large number of observations of tidal temperature and horizontal winds; in additions, observations show the impact of the tide on trace species (Marsh and Russell 2000; Smith et al. 2010a) and interactions with other waves (Chang et al. 2011). Figure 8 shows the temperature amplitude of the average diurnal tide near the March equinox derived from SABER observations. The WACCM simulations of the amplitudes of temperature and zonal and meridional winds are shown in Fig. 9. The maximum amplitude in temperature occurs at

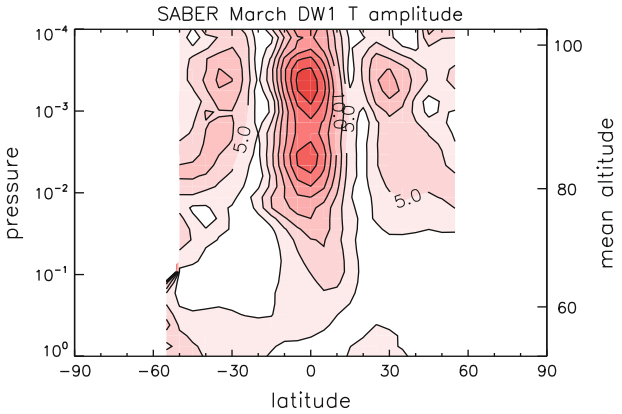

Fig. 8 Temperature amplitude of the migrating diurnal tide observed by SABER averaged over 2002–2011 for a 62-day period centered on March. Contour interval is 2.5 K

the equator while the maxima in horizontal wind occur around ±20° latitude. It is evident from a comparison of the WACCM and SABER temperature amplitudes that WACCM underestimates the amplitude of the tide. The reason for this is currently under investigation.

The seasonal variation determined from long-term MF radar wind measurements of the MLT by Vincent et al. (1988, 1998) and Fritts and Isler (1994) shows a March/April tidal amplitude maximum. Strong seasonal variations have also been documented from winds observed by HRDI (Burrage et al. 1995; Lieberman 1993; Huang and Reber 2003), by WINDII (McLandress et al. 1996), and by TIDI (Wu et al. 2008). Variations in the diurnal tide in temperature were documented from SABER by Zhang et al. (2006) and Xu et al. (2009b). The satellite record agrees with the seasonal variation found in radar data: amplitude of the DW1 tide in low latitudes is largest during equinoxes. The semiannual variation in tidal amplitude is simulated in global models, including WACCM (shown in Fig. 10).

Various explanations have been proposed for the equinoctial maximum. The proposed mechanisms fall into three categories: semiannual variations in the heating that forces the tide, variations based on the background winds in the tropical stratosphere or mesosphere, and variations due to damping within the middle atmosphere. The tropospheric heating projected onto the leading symmetric Hough mode has maximum during the December solstice period while the heating projected onto the first asymmetric mode has an equinoctial maxima (Lieberman et al. 2003). The magnitude of the seasonal variations in the heating due to absorption of sunlight by water vapor in the troposphere is small compared with the observed seasonal variations in DW1 amplitude. Hagan and Forbes (2002) found that forcing of DW1 by latent heat release in the troposphere has a pronounced semiannual variation with maximum forcing in the equinox months. The diurnal tide forcing by ozone heating in the stratosphere also has seasonal variations (Xu et al. 2010). In this case, maximum forcing of the leading symmetric Hough mode occurs during NH winter. Taken together, the seasonal variations in water vapor heating in the troposphere and ozone heating in the stratosphere do not provide support for the heating being the cause of the observed seasonal cycle in tidal amplitude. On the other hand, seasonal variations of latent heat release are consistent with the observed changes in tidal amplitude and may contribute to the seasonal cycle. Achatz et al. (2008) looked at the possibility that planetary wave

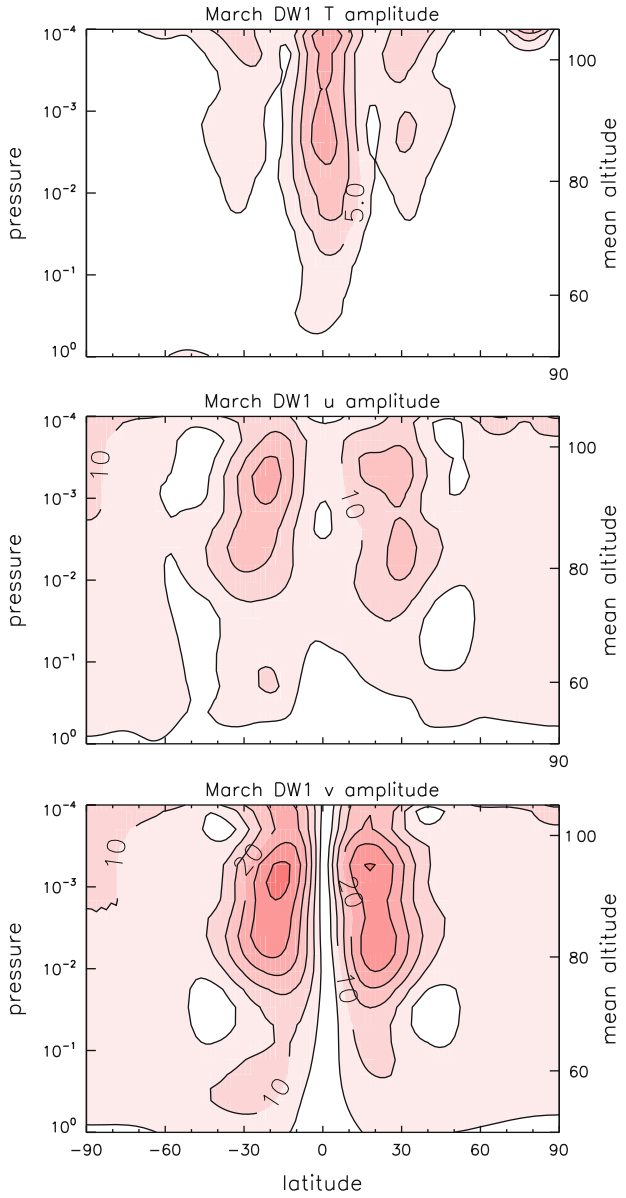

Fig. 9 Temperature, zonal wind, and meridional wind amplitudes of the migrating diurnal tide simulated by WACCM averaged over 1960–2006 for March. Contour interval is 2.5 K for the top panel and 5 m/s for the *center* and *bottom panels*

interactions affect the annual cycle of the migrating diurnal tide; they found that these have no important impact.

A second proposed explanation for the observed seasonal cycle is that the tidal propagation is affected by the zonal winds through which the tide propagates. McLandress (2002a, b) showed in the CMAM model that the tide varied based on the zonal winds in the

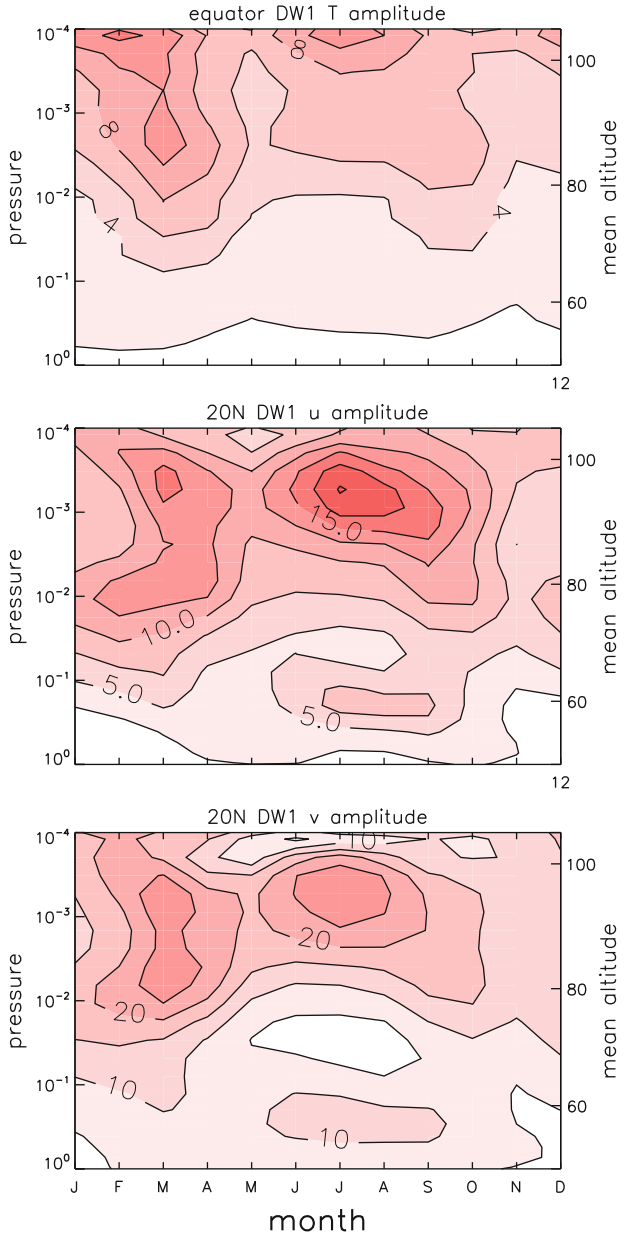

Fig. 10 Annual variation in monthly mean amplitude of the migrating diurnal tide temperature at the equator and zonal and meridional wind at 20°N from WACCM climatology. Contour intervals are 2 K for the *top panel*, 2.5 m/s for the *center panel*, and 5 m/s for the *bottom panel*

middle atmosphere. His analysis showed that there is a strong semiannual variation in the latitudinal gradient of the zonal wind in low latitudes. This gradient introduces a vorticity that is comparable in magnitude to the Coriolis torque and affects the tidal amplitude. In

the model, the semiannual variation in net tidal heating also contributed to the simulated seasonal cycle in tidal amplitude.

A third factor to consider is the possibility that tidal damping is larger during the solstice seasons, leading to maximum amplitude during the equinoxes. Analysis of satellite observations by Xu et al. (2009a) show that the damping of the DW1 tide by gravity wave interactions is largest when the tide itself is largest, thus indicating that damping is not responsible for causing the tidal seasonal cycle. Using different analysis of the same satellite observations, Lieberman et al. (2010) came to a different conclusion that the gravity wave interactions affected mainly the DW1 phase and not the amplitude. Neither of these analyses provides evidence that damping by gravity wave interactions is the primary cause of the seasonal cycle in DW1.

A periodicity that appears in investigations of the interannual variability of the DW1 tide is a biennial or quasi-biennial oscillation (QBO) (Burrage et al. 1995; Wu et al. 2008; Xu et al. 2009b). The amplitude of the DW1 tide varies in alternate years and appears to be related to the QBO in the zonal wind in the lower stratosphere. The tidal QBO is most apparent as a variation in the amplitude during the NH vernal equinox season (March/April). It is this link between the interannual and seasonal variations that makes it difficult to distinguish between a biennial or QBO variation when only a limited number of years of data is available. The phase of the tidal QBO is such that the March tidal amplitude is larger when the equatorial zonal wind at 30 hPa is eastward. Explanations for the interannual variability are still not agreed on. They are similar to those for the seasonal cycle except it is evident that variations of the sources within the troposphere do not contribute to the QBO. In a mechanistic numerical model, Mayr and Mengel (2005) found that filtering of gravity waves by winds in the stratosphere was able to transfer the QBO signal to the MLT. It is also possible that winds in the lower stratosphere affect the tidal forcing but mechanisms have not been identified.

Although WACCM version 3.5 does not self-generate a QBO in the lower stratosphere, QBO wind variations are imposed by applying a slowly varying forcing in the tropics between 100 and 10 hPa (Richter et al. 2011). The timing and amplitude of the QBO forcing varies from month to month based on observations. Figure 11 shows a scatter plot of the WACCM meridional wind tidal amplitude at 20°N and 90 km in March versus the zonally averaged zonal wind at the equator at 24 hPa. The figure shows a clear relationship between the tidal amplitude in the MLT and the lower stratospheric QBO. The tidal amplitude is never large during the easterly phase of the QBO. During the westerly phase, the amplitude is more variable and can be much larger. The phase of the QBO in WACCM tides agrees with that observed.

Lieberman et al. (2007) investigated the response of the DW1 tide to large-scale interannual changes in the diurnal component of tropospheric water heating associated with an El Niño event in the tropical ocean/atmosphere. The heating changes include both the absorption of radiation by water vapor and latent heat release. They found that the heating changes during 1997–1998 were sufficient to account for a maximum in the diurnal tide amplitude that was observed in low latitudes during that period.

4.3.2 Semidiurnal and Higher-Frequency Tides

The horizontal wind amplitudes of the migrating semidiurnal tide, SW2, tend to be largest in middle to high latitudes (Pancheva et al. 2009a), so they can be the dominant tidal signal in these areas. The latitude differences between the diurnal and semidiurnal tides are readily explained by the Hough mode structures. The heating projects best onto the gravest

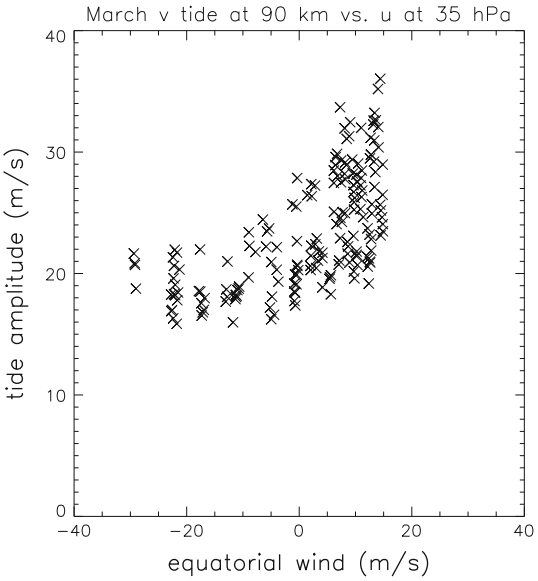

Fig. 11 Scatter plot showing the WACCM meridional wind amplitude of the migrating diurnal tide during March at 20°N and 0.0015 hPa (about 90 km) versus the equatorial stratospheric zonal mean zonal wind at 35 hPa (22 km). Units for both are m/s

symmetric Hough mode which, for DW1 temperature, approaches zero in high latitudes. In contrast, the gravest symmetric Hough mode for SW2 extends from pole to pole.

The maximum amplitude of the SW2 tide tends to be above the mesopause, whereas that of the DW1 tide is around 95 km. This difference is likely related to the vertical structure. DW1 has a relatively short vertical wavelength of $\sim$25 km. This leads to stronger interactions with gravity waves and therefore to stronger damping. Observations indicate that the vertical wavelength of SW2 varies with latitude and season but even the lowest values observed (35 km found by Pancheva et al. 2009a) are longer than that of DW1. A longer vertical wavelength reduces the magnitude of wind and temperature gradients due to the tide and makes it less susceptible to damping by gravity wave interactions.

Figure 12 shows the multiyear average temperature semidiurnal tide from SABER for 60-day periods centered on December. The WACCM climatological temperature amplitude for December is shown in Fig. 13, along with the horizontal wind amplitudes. The SABER and WACCM amplitudes are similar at the highest level shown (10^{-4} hPa) but the amplitude simulated by WACCM is not as large below there. SABER amplitude of >5 K occurs down to 3×10^{-3} hPa in both hemispheres whereas, in the WACCM simulations, such amplitudes are seen only above 4×10^{-4} hPa.

Analysis of lidar observations at a site in NH midlatitudes by Yuan et al. (2008) indicates that the semidiurnal tide shows seasonal variations in the phase structure. At this site, the tide is vertically propagating during winter and equinox periods and has a vertical wavelength ranging from 50 to 90 km. During summer, the wavelength becomes even longer or becomes evanescent (no wave-like structure in the vertical profile). Yuan et al. (2008) interpret the seasonal changes as resulting from a different superposition of migrating and nonmigrating modes during the different seasons.

While most work has focussed on the diurnal (24-h) and semidiurnal (12-h) tides, higher-frequency tides have also been observed. Taylor et al. (1999) reported a large amplitude terdiurnal (8-h) tide in temperature data from an airglow imager. Younger et al.

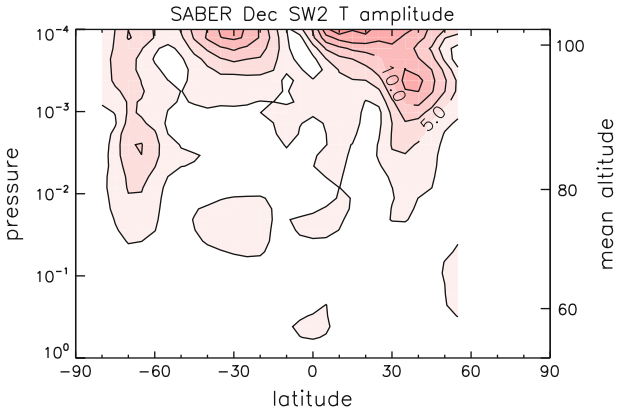

Fig. 12 Temperature amplitude of the migrating semidiurnal tide observed by SABER averaged over 2002–2011 for a 62-day period centered on December. Contour interval is 2.5 K

(2002) showed the terdiurnal tide in radar winds at 68°N. Smith (2000) and Du and Ward (2005) presented the global and seasonal structure of the terdiurnal tide in horizontal winds observed by HRDI and WINDII, respectively. Modeling studies by Smith and Ortland (2001) and Akmaev (2001a) indicated that the mean terdiurnal tide is primarily forced by solar heating although generation by nonlinear interaction between diurnal and semidiurnal migrating tides also contributed.

Tides with even higher frequency are seen in radar observations. For example, Smith et al. (2004) presented observations and modeling of a 6-h tide. Analysis of the high-frequency tides from observations made with a precessing satellite is a challenge because small changes in the amplitude or phase of lower-frequency tides (particularly diurnal and semidiurnal) can affect the analysis.

4.3.3 Nonmigrating Tides

Numerous observations indicate that nonmigrating diurnal (Oberheide et al. 2005, 2006) and semidiurnal (Baumgaertner et al. 2005; Murphy et al. 2006) tides are normal phenomena of the MLT. Nonmigrating tides can be excited by longitudinal variations in the diurnal heating. The most obvious source of heating variations is latent heat release in the tropical region (Hagan and Forbes 2002; Hagan et al. 2009). The presence of a DE3 tide has been attributed to the heating distribution, in particular to the alternating high and low rates of latent heat release due to the alternating continents and ocean with longitude in the equatorial region (Hagan et al. 2009; Akmaev et al. 2008).

Nonmigrating tides can also be excited by nonlinear interactions between the migrating tides and quasi-stationary planetary waves (Oberheide et al. 2002; Lieberman et al. 2004). A nonlinear interaction between two large-scale waves (the parent waves) can produce child waves with related structure. The wavenumber and frequency of the child waves must be the sum or difference of the wavenumbers and frequencies of the parent waves. This mechanism can produce migrating tides as well. For example, the interaction of DW1 and SW2 can generate the migrating terdiurnal tide. Non-migrating tides can be produced by the interaction of migrating tides with planetary waves. The dominant planetary waves in

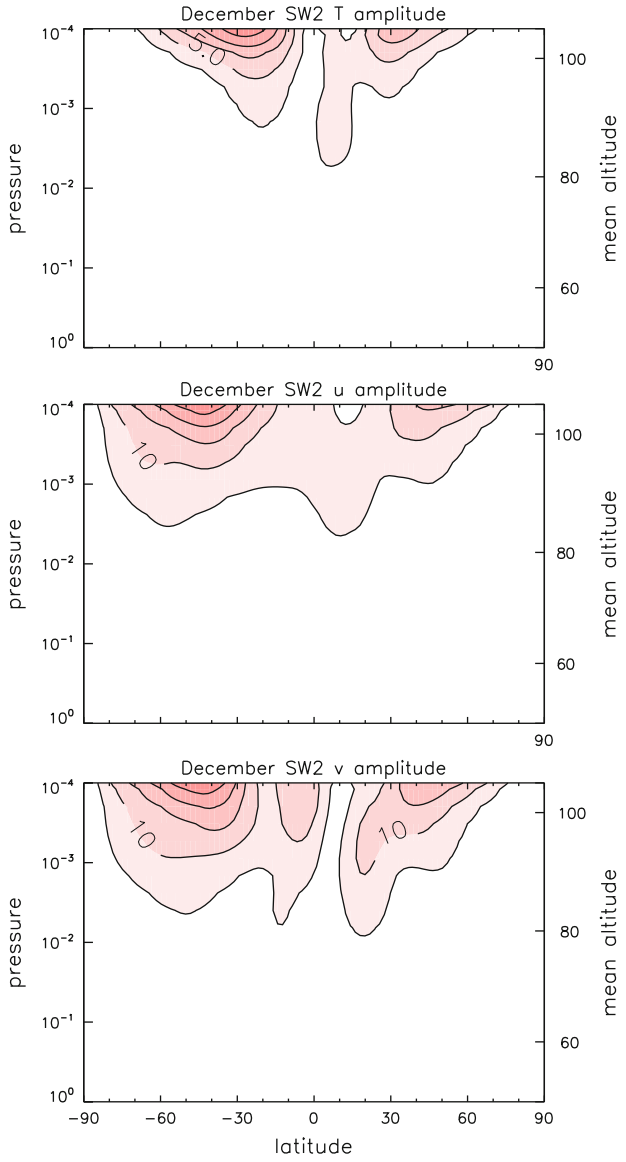

Fig. 13 Temperature, zonal wind, and meridional wind amplitudes of the migrating semidiurnal tide simulated by WACCM averaged over 1960–2006 for December. Contour interval is 2.5 K for the *top panel* and 5 m/s for the *center* and *bottom panels*

the winter stratosphere are quasi-stationary with low zonal wavenumbers (wavenumbers 1 and 2 are the largest); a quasi-two day wave with zonal wavenumber of 3 or 4 is often seen in the mesosphere.

Figure 14 shows a wavenumber breakdown of the climatological diurnal tide simulated in WACCM for October at 95 km. The migrating tide (DW1) is clearly prominent. Also

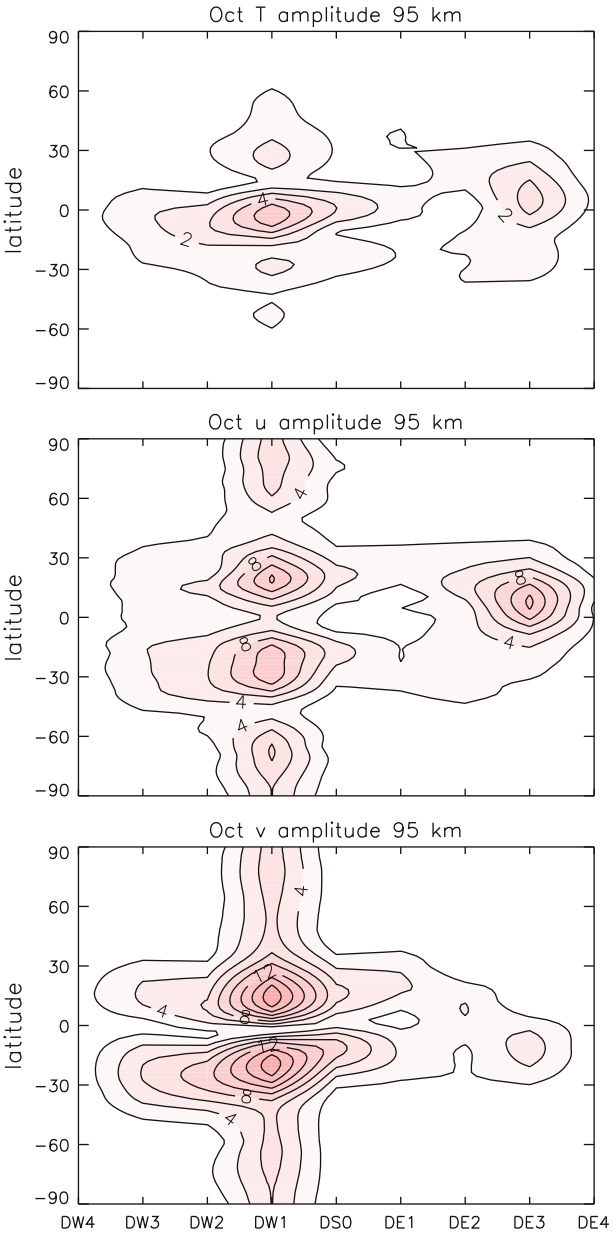

Fig. 14 October mean amplitude of the diurnal tide as a function of zonal wavenumber and latitude at 95 km from WACCM climatology. Contour interval is 1 K for the *top panel* and 2 m/s for the *center* and *bottom panels*

note the large DE3 tide during this month. Other modes that have appreciable amplitude are DW3, DW2, and DS0. The simulated temperature tide in high southern latitudes is smaller than that observed by lidar during January 2011 (Lübken et al. 2011).

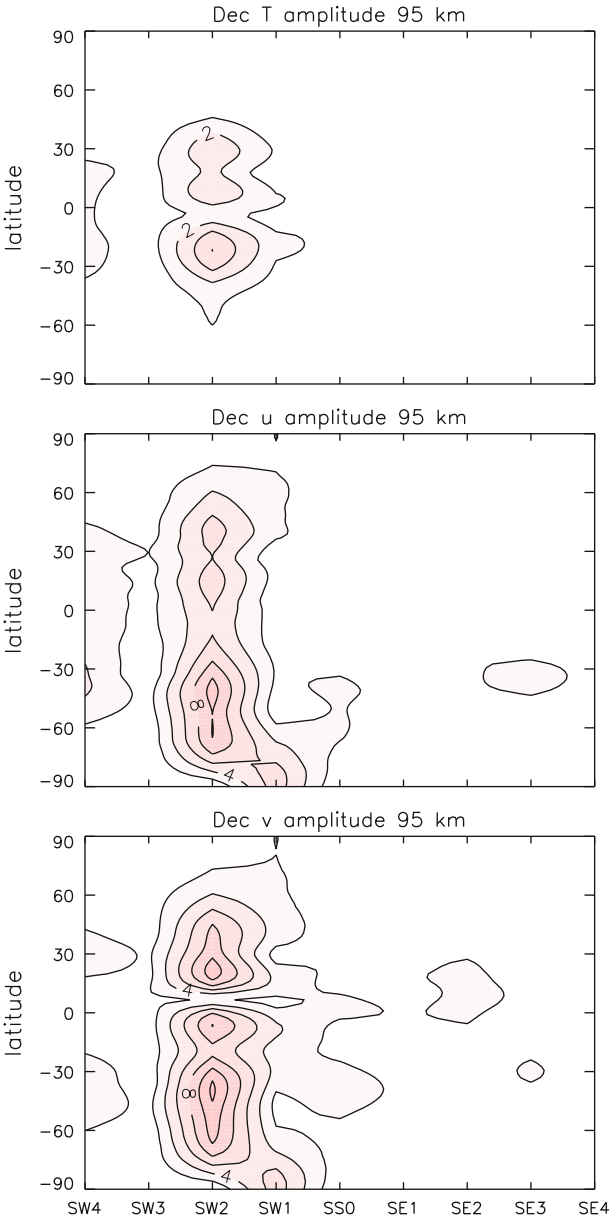

Fig. 15 As in Figure 14 but for the semidiurnal tide in December

Observations of tidal motion at the South Pole (Portnyagin et al. 1998) find a persistent SW1 tide in meridional wind during the summer months. Calculations by Forbes et al. (1995) and Angelats i Coll and Forbes (2002) indicate that nonlinear interaction between SW2 and a stationary planetary wave with zonal wavenumber 1 can generate two waves, the nonmigrating semidiurnal tides SW1 and SW3. The SW1 tide is also seen in WACCM,

as shown in Fig. 15, although its amplitude is weaker than observed. The SW3 tide that has been observed in Antarctica does not appear in the WACCM simulations. Note that the interaction between the migrating semidiurnal tide and planetary wave can also decrease the amplitude of the SW2 tide, one of the parent waves (e.g., Chang et al. 2009).

Observations (Baumgaertner et al. 2005; Murphy et al. 2009) indicate that the SW1 tide is present around the perimeter of Antarctica. Murphy et al. (2009) showed that the temporal variations in SW1 were well correlated with variations in the amplitude of stationary planetary wave 1 in the NH. They also found a link between SW3 and the NH planetary wave. While not conclusive, this robust correlation provides good evidence that the SW1 in the southern summer MLT is caused by a nonlinear interaction between SW2 and a stationary planetary wave 1 in the stratosphere of the winter hemisphere. The relationship can also go in the opposite direction, from the SH winter to the NH summer. Smith et al. (2007) found a correlation between the planetary wave amplitude in the SH at the semidiurnal tide at a single radar site in the NH. In their analysis, with data from a single site, it was not possible to distinguish between the migrating and nonmigrating semidiurnal tides.

The interaction of tides with planetary waves can also generate nonmigrating tidal modes that are seen locally (in the same hemisphere or even at the same latitude as the planetary wave). Such responses were seen by Liu et al. (2007) in northern midlatitudes and Baumgaertner et al. (2006) in the southern hemisphere.

4.4 Planetary Waves

The term planetary waves refers to various phenomena, some of which are components of middle atmosphere dynamics. In general terms, planetary waves are propagating large-scale disturbances with low zonal wavenumbers. Conservation of angular momentum is the restoring force that governs the wave dynamics.

Quasi-stationary Rossby waves are the dominant disturbances in the extratropical winter stratosphere and lower mesosphere. Stationary Rossby waves with low zonal wavenumbers (typically wavenumbers 1–3) can propagate vertically where the background zonally averaged zonal wind is westerly (Charney and Drazin 1961). This condition is usually met in the winter stratosphere and lower mesosphere. The wintertime zonal wind may reverse from westerly to easterly in the upper mesosphere; the altitude where the reversal occurs varies with latitude, season, and can have large interannual variations due to dynamical activity. Quasi-stationary waves are difficult to separate from the background winds and temperatures in radar and lidar observations but can be observed by satellite. Mukhtarov et al. (2010) present observations of the stationary waves in temperature observed by the SABER satellite instrument. The amplitudes are small in the region of the mesopause ($\sim$100 km altitude).

A planetary-scale variation in the small-scale waves that propagate into the mesosphere can exist due to planetary-scale variations in the generation of the small-scale waves. Another means of generating variations is through differences in the filtering or dissipation of the waves due to the differences in winds, temperature, etc. As shown by Smith (2003), planetary waves in stratospheric winds can filter the gravity waves propagating from below, leading to large-scale variations in the gravity wave flux that propagates into the MLT. When the gravity waves break or dissipate, they will generate a planetary wave pattern in the MLT winds and temperature. Quasi-stationary planetary waves have been seen in the winter MLT (1996, 1997; Wang et al. 2000; Xiao et al. 2009). These probably

contain a mix of planetary scale disturbances that have propagated from lower altitudes and wavelike variations due to interactions with small scale waves.

Quasi-stationary planetary waves are absent in the summer stratosphere. Normally during the solstice seasons, the mean zonal winds reverse in the mesosphere; the result is westerly winds in summer and easterly winds during winter. As shown originally by Dickinson (1968), under some circumstances, there can be continuous westerly winds across the tropics from the winter stratosphere to the summer mesosphere. This phenomenon known as the mesospheric tropical waveguide, creates a path for propagation of quasi-stationary planetary waves into the summer mesosphere. Depending on characteristics of the winds and waves, the waveguide can also allow the propagation of other waves (for example, planetary waves with nonzero frequency).

The tropical waveguide has been seen in the observations of the zonal wind (e.g., McLandress et al. 1996; Fleming et al. 1996). Wang et al. (2000) and Garcia et al. (2005) reported the observations of stationary planetary waves in the summer mesosphere in winds and temperature, respectively. Forbes et al. (2002) investigated the source of summer waves observed in the MLT and concluded that the propagation of waves from the winter hemisphere was a likely explanation for the presence of the waves in the summer hemisphere.

Traveling planetary-scale waves can achieve high amplitude in the MLT. The periods of traveling waves cluster around periods associated with atmospheric normal modes. One commonly observed mode is the quasi-two day wave, which has a period of about 2 days and a zonal wavenumber of 3 or 4. It is regularly observed in the mesosphere just after solstices and can attain very large amplitudes (meridional wind ~ 30 m/s) (Riggin et al. 2004; Limpasuvan and Wu 2009; Offermann et al. 2011a). Other commonly reported periods are 5 day (Riggin et al. 2006), 6.5 day (Lieberman et al. 2003; Liu et al. 2004), 10 day, and 16 day (Day and Mitchell 2010). These waves do not directly transport much momentum. However, they can interact with other waves such as quasi-stationary Rossby waves, gravity waves, and tides and thereby affect the momentum budget and the periodicity of variability in the middle atmosphere. Spectral breakdown of planetary waves in mesospheric observations has been given by Garcia et al. (2005) and Pancheva et al. (2008, 2009b, c).

Equatorially trapped waves are, as the name indicates, limited to the tropics. These waves fall into two categories: Kelvin waves, which propagate eastward, and mixed-Rossby gravity waves, which propagate westward. Planetary-scale Kelvin waves with short periods have large vertical wavelengths. These waves are less rapidly damped in the middle atmosphere than are Kelvin waves with shorter vertical wavelengths. They are also less likely to be dissipated by critical line interactions because of their fast phase speeds. Salby et al. (1984) showed the presence of very fast Kelvin waves in the upper mesosphere. Numerous observations confirm that these waves are a frequent feature of the tropical MLT (e.g., Younger and Mitchell 2006; Takahashi et al. 2007; Forbes et al. 2009; Chang et al. 2010). Kelvin waves with periods of 24 hours contribute to the observed spectrum of eastward propagating tidal motions.

5 Vertical Coupling Between the Stratosphere and MLT

5.1 MLT Variations due to Active Winter Dynamics

Model predictions and observations indicating the interaction of the stratosphere with the MLT during dynamically active winter periods have a long history. Characteristic variations to the mesosphere are associated with strong disturbance in the stratosphere. One topic of

particular interest is the MLT response to stratospheric sudden warmings (SSWs). SSWs are extreme events in which there is rapid warming of the polar stratosphere and reversal of the normally westerly winds to easterly in the middle stratosphere. They are caused by interaction of planetary waves with the stratospheric mean flow. Frequent SSWs in the years since 2000 (Charlton and Polvani 2007) have provided opportunity for extensive observations of the MLT response. It is well documented that the symptoms of SSWs are first seen at higher altitudes in the mesosphere and propagate downward over a period of a few days.

Ground-based observations of MLT winds and temperature (Hoffmann et al. 2007) showed clear wind perturbations up to the highest level shown, about 90 km. The observations also indicate that the perturbations in the stratospheric zonal wind affect gravity wave propagation into the MLT. Siskind et al. (2005) found from SABER temperature observations that the mesospheric cooling associated with the stratospheric warming events was confined to the levels below about 85–95 km.

The response through the depth of the middle atmosphere was simulated by Liu and Roble (2002). Their model study showed a broad region of negative temperature perturbation extending to about 110 km that coincides with the stratospheric warming. Using a version of the same model, Yamashita et al. (2010) showed that the simulated MLT response to a SSW was sensitive to the settings in the gravity wave parameterization. The settings influence the model simulation of planetary wave propagation and damping. They can also affect the vertical structure of the MLT response to the stratospheric perturbations, including the vertical domain over which cooling is simulated.

Global observations extending from the lower stratosphere into the upper mesosphere have enabled the documentation of several important ways in which variability in the MLT is driven by variability in the winter stratosphere. Much attention was focused on this topic due to surges of certain trace chemicals into the high latitude middle atmosphere during some active periods during 2004, 2006, and 2009. The flux of tracers was a signature of rapid downwelling from the MLT region to much lower altitudes. These three winter periods all followed strong midwinter SSWs. However, the persistence of an altered state and strong downward transport during the winter occurs only after some, not all, SSWs.

A striking aspect of the unusual dynamics of those winters were shown in the observations of temperature (Manney et al. 2005, 2008, 2009; Orsolini et al. 2010) and simulations of similar events by WACCM (Chandran et al. 2011; Limpasuvan et al. 2011). In those winters, the position of the stratopause, identified as the middle atmosphere temperature maximum, jumped from its average altitude range (45–55 km) to 75–85 km. The warm temperature in the upper mesosphere was a response to downwelling by increased gravity wave activity while the cooler temperatures below indicated gravity wave breaking in that region was suppressed. Observations also indicated perturbations to the distributions of chemical species that are produced in the MLT (e.g., Randall et al. 2009; Smith et al. 2009a; Kvissel et al. 2012).

Because of the limited availability of satellite observations spanning the lower to upper mesosphere in winter high latitudes, the observational record showing the response of the MLT to winter dynamics is still incomplete. Models and analysis of observations point to the importance of gravity waves and their filtering by stratospheric winds in the vertical coupling in this region. This once again highlights the challenges for global models and observations.

5.2 Summer MLT

The changing climate in high southern latitudes, particularly the deep and persistent spring ozone hole over Antarctica, has led to later breakdown of the winter westerly vortex in the

SH (Karpetchko et al. 2005; Haigh and Roscoe 2009; Eyring et al. 2010; WMO 2010). The temperature in the lower stratosphere during spring has become lower (Thompson and Solomon 2002; Randel et al. 2009) and the winds more westerly. In the analysis of WACCM by Smith et al. (2010b), the stratospheric changes affected propagation of gravity waves from the troposphere to the mesosphere. On a long (multiyear) timescale, the trend in the temperature at the early summer mesopause (November and December) was traced to the ozone hole development. Lossow et al. (2012) found a similar perturbation in the CMAM model although in that model the trend was seen only during November. Observational confirmation of the relationship, albeit on a shorter interannual timescale, was provided by Hernandez (2004), who found a relationship between the MLT temperature at the South Pole and the size of the Antarctic ozone hole.

On short timescales of a few days, ozone in the stratosphere is affected by dynamics through transport and temperature-dependent photochemistry. The feedback of the ozone changes on dynamics through changes in radiative forcing is not important on this timescale because the radiative timescale is more than a week (Shine 1987). On the other hand, the persistence of a remnant of the winter vortex in the SH long after spring equinox, and even to the summer solstice (Black and McDaniel 2007), could affect the summertime mesospheric circulation. This is because both the mean winds and the planetary waves in the stratosphere affect the propagation of gravity waves that, in turn, drive the mesospheric circulation.

Variations in the timing of the SH stratospheric vortex breakdown introduce a source of variability that can influence the summer mesopause in the SH. Kirkwood et al. (2008) reported a higher position for the mesopause during Novemeber 2007; they attributed this anomaly to the filtering of gravity waves by winds in the middle atmosphere. Gumbel and Karlsson (2011) found that the onset of the season for polar mesospheric clouds in the SH summer of 2010–2011 was delayed by several weeks. This coincided with a delayed breakdown of the westerly jet in the stratosphere during this summer season. The delayed vortex breakdown has important impacts on the filtering of gravity waves that drive the circulation in the mesosphere (e.g., Smith et al. 2011). The eastward gravity waves that drive the upwelling branch of the circulation cannot propagate under these conditions. Adiabatic cooling associated with the upwelling is responsible for cooling the summer mesopause; changes in the gravity wave driving will therefore affect the temperature in the MLT.

The persistence of westerly winds in the stratosphere over Antarctica into the spring and even early summer means also that planetary waves can exist later in the season. Zonal asymmetries in the winds in the stratosphere may, through the filtering of gravity waves, also lead to zonal asymmetries in the wave flux into the mesosphere, as discussed in Sect. 4.4

6 Hemispheric Differences and Interhemispheric Teleconnections

6.1 Interhemispheric Teleconnections

In recent years, some surprising aspects of global teleconnections in the middle atmosphere have come to light. Two phenomena involving the impact that winter variability in the stratosphere has on the upper mesosphere of the summer hemisphere have been documented. In one case, the signal is seen in semidiurnal nonmigrating tides and, in the other, it is evident in mean winds, temperature, and polar mesospheric cloud occurrence frequency. Although both signals are related to dynamical variability in the winter

stratosphere, there has been no indication that the hemispheric teleconnection in tides is otherwise related to that in the time-mean fields.

6.1.1 Teleconnections Involving Tides

The dynamics in the northern hemisphere (NH) winter stratosphere are quite variable. Planetary waves and the zonal mean wind and temperature all vary in response to dynamical perturbations propagating from the troposphere. The variations in planetary wave amplitude are correlated with variations in the amplitude of migrating semidiurnal tides in high southern latitudes (Murphy et al. 2009). Since variations in the wave amplitudes, the mean wind, and the temperature in the winter stratosphere are well correlated, observations cannot give a definitive answer about which of these contribute to the tidal response. Smith et al. (2007) observed a similar correlation between NH summer tides and planetary waves in the SH.

There are numerous observations of the nonmigrating SW1 mode in the SH (e.g., Forbes et al. 1995; Portnyagin et al. 1998; Murphy et al. 2003, 2006; Aso 2007; Chang et al. 2009; Hibbins et al. 2010; Iimura et al. 2009). Yamashita et al. (2002) reproduced the relationship between the SH semidiurnal nonmigrating tides and the NH stratospheric planetary waves in an atmospheric circulation model. In their model, Eliassen-Palm fluxes indicated propagation of nonmigrating tides from the winter stratosphere toward the summer mesosphere. Simulation of a sudden stratospheric warming by Liu and Roble (2002) also shows the generation of nonmigrating semidiurnal tides by interaction of a planetary wave with the migrating tide. Xu et al. (2009d) found a correlation between the SH semidiurnal tide measured by radar and the planetary wave 1 in the NH winter but did not find a comparable correlation between the NH semidiurnal tide and the SH winter planetary wave 1. They did not have enough information to separate the tidal variations into migrating and nonmigrating contributions, so the hemispheric comparisons are likely affected by the longitudes of the radars used to determine the tidal variations.

6.1.2 Teleconnections Involving Zonal Mean Winds and Planetary Waves

A teleconnection pattern has also been seen that involves mean states (zonally averaged temperature or zonal winds), planetary waves, and the characteristics or occurrence frequency of polar mesospheric clouds (PMCs). The wintertime variations in planetary waves and the background zonal mean temperature, winds, and circulation are closely coupled. Therefore, it is not possible, using observations or complex general circulation models, to separate the effect of variability of stratospheric planetary waves (such as wave–wave interactions) from those of the mean temperature and winds (such as filtering of gravity waves by the stratospheric winds). The winds and temperature in the winter stratosphere are highly correlated with the waves on multiple timescales (Xu et al. 2009c). Becker et al. (2004) and Becker and Fritts (2006) used model simulations to show that temperature changes observed in the NH summer mesopause were related to dynamical events in the SH winter. Karlsson et al. (2009a) analyzed simulations from the Canadian Middle Atmosphere Model and found that the model reproduces the observed relationship. Karlsson et al. (2007, 2009b) found a link between variability of PMCs and dynamical variations in the opposite (winter) hemisphere stratosphere. Espy et al. (2011) found that the correlation varied with the phase of the QBO in tropical stratospheric zonal wind.

Calculations do not support a direct connection through a global circulation driven by winter planetary waves or by gravity waves that have been filtered by the planetary waves

or the associated changes in stratospheric mean wind. While such a circulation could cause upwelling in the tropics, the extension to the summer pole is not supported. Likewise, direct propagation of planetary waves from the winter to summer hemisphere has not been invoked as a primary mechanism in the published studies although propagation of planetary waves into the summer midlatitude MLT has been seen in both observations and models. The mechanism proposed to explain model simulations of the teleconnection pattern (Becker and Fritts 2006; Karlsson et al. 2009a; Kornich and Becker 2010) involves feedbacks among the mean circulation in the latitude-height plane, gravity wave propagation and breaking, and the zonally averaged wind.

To follow this mechanism, consider a case where the stratospheric polar temperature is higher and the zonal wind is weaker than the climatological values. This corresponds to a period of active dynamics, driven by large transient planetary waves and wave-mean flow interaction in the stratosphere. The weak zonal wind in the stratosphere affects the filtering of gravity waves, with the result that the net momentum forcing in the MLT is weaker than the climatological values. This in turn leads to a weaker driving of the poleward circulation in the MLT that brings midlatitude air toward the pole (see Fig. 4). The weaker circulation affects the rising motion in low latitudes and reduces the adiabatic cooling, thus increasing the temperature in the tropical MLT. The increased tropical temperature then increases the temperature gradient between the cold summer pole and the tropics and, through the thermal wind relation, strengthens the summer westerly winds in the MLT. This affects the gravity wave interactions in the summer hemisphere and reduces the driving of the equatorward circulation there. Through changes in the strength of the adiabatic cooling, there is a positive perturbation to the mean temperature in the poles that correlates with the temperature perturbation in the winter stratosphere. Using a simple model, Kornich and Becker (2010) were able to document each of the steps that give rise to this teleconnection pattern.

6.2 Hemispheric Differences

The winds in the winter stratosphere are stronger in the SH, due in large part to weaker quasi-stationary planetary waves that propagate from the troposphere. The stronger eastward winds affect the propagation of gravity waves with westward phase speeds and the filtering of gravity waves with eastward phase speeds. When the gravity waves break or dissipate near the stratopause or in the mesosphere, the net momentum forcing will then be stronger in the SH. This winter difference leads to a stronger circulation in the SH and to a higher winter mesopause temperature. Planetary waves do not play an important role in the summer stratosphere but, nevertheless, there are also hemispheric differences in the stratospheric summer zonal winds.

Both the height and temperature of the mesopause in high-latitude summer have differences between the two hemispheres. As described in Sect. 3, the low temperature and low altitude of the summer mesopause is due to very strong upwelling near the pole. The summer mesopause is colder and at a lower altitude in the NH summer compared to the SH summer (Huaman and Balsley 1999). Chu (2003) and Chu et al. (2006) reported hemispheric differences of about 1 km in the altitude of polar mesospheric clouds (PMC) from lidar measurement. PMC altitudes are sensitive to temperature but also to other variable fields such as water vapor and vertical wind. Xu et al. (2007a) found similar differences in the mesopause height determined from SABER temperature measurements. Hervig and Siskind (2006) found larger differences in mean summer temperature at $65-70^\circ$ in HALOE data; the SH was warmer by 3–6 K throughout the mesosphere.

The hemispheric asymmetries in mesopause temperatures and altitudes can be seen in Fig. 1, upper panels. This difference is not well simulated in WACCM (Fig. 1, lower panels); the minimum summer temperatures reached in the two hemispheres are similar, but the simulated mesopause altitude is higher during NH summer. Siskind et al. (2003) reported a stronger gravity wave-driven circulation in the NH during July than in the SH during January in simulations using a two-dimensional model, consistent with the WACCM results for those months.

The annual variation in Earth–Sun distance (closest during January) leads to a solar flux change of about 6 %. This difference can also affect hemispheric differences, including the mesopause temperature and altitude (Chu 2003). Simulations made with the thermosphere–ionosphere–mesosphere-electrodynamics global climate model (TIME-GCM) indicated that the mesopause difference is mainly caused by the solar flux differences between January and July (Chu 2003).

Dowdy et al. (2001, 2007) presented hemispheric differences in high-latitude zonal and meridional wind measured by radar (two sites in each hemisphere). They found that winter zonal winds in the SH were stronger and their seasonal variations were more symmetric around the winter solstice than were those in the NH.

Tidal motions also have hemispheric differences that are apparent in global analyses that show the amplitudes in both hemispheres (e.g., McLandress et al. 1996; Xu et al. 2009b; Pancheva et al. 2009a). Pancheva et al. (2009a) noted that the seasonal cycles in the SW2 tidal temperature amplitudes determined from SABER observations are not symmetric. At 90 km, the amplitude of SW2 at both 40°N and 40°S has an annual cycle, but the NH maximum is in winter (December–February) while the SH maximum is in late fall (May). Hemispheric differences in tides are also simulated in global models (for example, see Fig. 9), but there has not been been much effort to catalog and explain these differences.

As discussed in Sect. 4.1, gravity waves are normally difficult to determine from global measurements. Much of the information about large-scale hemispheric differences in MLT gravity waves comes from inferences in global models, particularly the impact of filtering by stratospheric winds. The impact of filtering is large and important, and it appears, to first order, to be well-simulated by the parameterizations in global models.

Although the filtering of gravity waves in the stratosphere is undoubtedly important, the gravity wave sources may also play a role. There are important gaps in knowledge about hemispheric differences in gravity wave sources and in the actual wave propagation (lateral as well as vertical). Coarse-resolution global models are a poor tool for addressing these issues. The new generation of high-resolution GCMs that resolve gravity wave generation and propagation, such as that described by Sato et al. (2009), will be a helpful tool in addressing this question.

On the other hand, interpretation of gravity wave observations by radars at selected NH and SH sites can be complicated because it is difficult to separate local factors from those affecting a broader area. With the limited number of observation sites available, it is not possible to determine to what extent differences such as seasonal changes are affected by the local surface topography, stratospheric planetary waves, etc., rather than the regional mean conditions. Dowdy et al. (2007) compared the gravity wave activity measured at high latitude radar stations in the NH and SH (two radar sites in each; separated in longitude). In both hemispheres, there was a strong seasonal change in wave activity but the seasonal cycles differed between sites and also with altitude. Overall there was a summer maximum in gravity wave activity at all four sites.

7 Trends and Variations on Multiyear Timescales

Trends in the basic state dynamical fields of the MLT are expected from three causes: changes in the composition of radiatively active gases, changes in wave fluxes from below, and changes in energy input associated with solar activity. Diagnosing of trends is affected by the short records of many observing systems and the high natural variability of the MLT.

The vertical structure of the atmosphere, and specifically the geometric altitude of a given pressure level, depends on the temperature of the entire column below that pressure. Because of this, aspects of the MLT are sensitive to large-scale changes below. Through the hydrostatic relation, the height

$$z = -\int_{p_s}^{p} RT/gdlnp,$$

where p_s is the surface pressure, R is the gas constant for dry atmosphere, and g is the acceleration of gravity. A lower temperature through the column gives a lower height for the same pressure interval. Warming or cooling in either the troposphere or stratosphere can have an impact on the column.

Changes in the relation between altitude and pressure have two important considerations. First, they can affect not just the magnitude but also the sign of changes and trends. This was shown by Akmaev and Fomichev (1998) in a simulation of the impact of increased CO_2 on the MLT. On a pressure surface, the January response at $\sim 10^{-3}$ hPa was weak cooling but when the analysis was performed on the nearby altitude surface of 100 km, the response was a warming. The mesopause is particularly sensitive to this because there is a sharp change in the vertical temperature gradient from weakly negative below to strongly positive above. This effect is illustrated in Fig. 16, which shows the annual temperature trends from WACCM on pressure and altitude grids. The trend for the period 1960–2005 was calculated from four realizations of the model using multiple linear regression that removes the seasonal cycle and fits the linear trend along with interannual changes due to the QBO, volcanic eruptions, and the solar cycle. It is evident from the figure that the trends as a function of altitude are more positive in the MLT than those as a function of pressure, particularly above the temperature minimum at the mesopause.

The second concern with the mismatch between pressure and altitude coordinates is the effect on comparisons between numerical models (usually with pressure as a vertical coordinate) and observations (many give profiles as a function of geometric altitude). A

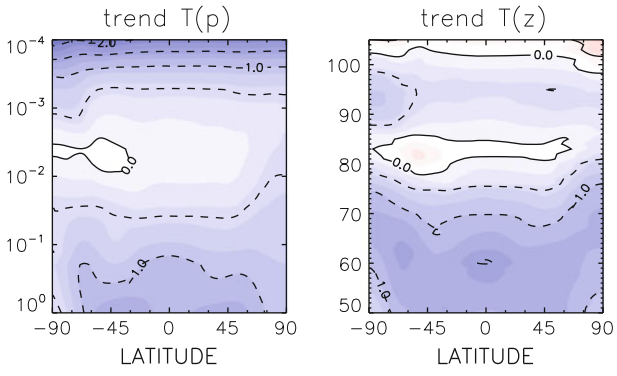

Fig. 16 Temperature trend simulated by WACCM for the period 1960–2005. *Left panel* is the trend on a log-pressure grid and *right panel* is the identical trend on an altitude grid. Contour interval is 0.5 K/decade

comparison that does not convert the vertical profiles to the same vertical coordinate system is not trustworthy and may be strongly misleading.

For most MLT observations, the trend analysis is affected by the relatively short observational record. Temperature, for example, is expected to be affected simultaneously by trends in anthropogenic greenhouse gases, changes in composition due to other tropospheric gases, and variations in solar flux and composition due to the solar cycle. Because of these competing or reinforcing processes, disentangling the drivers of the trends and variations is not possible using observations alone. While model simulations have their own problems, they are invaluable in giving guidance about the magnitude and basic structure of the mesospheric response to various applied changes.

7.1 Long-term Trends

Attributing changes in the MLT temperature to composition or other changes must be done carefully. One challenge, as discussed above, is the change in the height of pressure surfaces with the temperature in the underlying column. This is particularly an issue for changes in greenhouse gases, whose effects are felt in the troposphere and entire middle atmosphere. Through a modification of the pressure/altitude relation, the influence of greenhouse gases that have negligible concentrations in the MLT, such as methane (CH_4) and CFC12 (CF_2Cl_2), could nevertheless be felt there. Likewise changes in stratospheric ozone can affect wave propagation (see Sect. 5.2) as well as the column temperature (Bremer and Peters 2008). These remote effects are not included in the list of anthropogenic gases that affect the MLT, given below.

Changes in composition can also directly affect the chemistry and radiative balance of the MLT. Several gases that are known to have undergone long-term changes can also affect the MLT basic structure or dynamics.

CO_2 Infrared emission by CO_2 is the most important cooling process in the MLT (Feofilov and Kutepov 2012). CO_2 radiative transfer also gives seasonal weak heating at the cold summer mesopause. Higher concentrations of CO_2 lead to higher cooling rates. The global tendency associated with this change is for an increase in CO_2 to cause increased cooling and lower temperatures.

CH_4 Methane is produced at the Earth's surface from natural and anthropogenic sources. Methane that is transported into the middle atmosphere is oxidized in the stratosphere and lower mesosphere. The hydrogen released forms water (two water molecules for each methane) and contributes about half of the total amount of water above the stratopause. Measurements indicate that methane in the lower atmosphere has been increasing in recent decades although the trend is not monotonic.

H_2O Photolysis of water is the main source of reactive hydrogen (HOx, defined as the sum of H, OH, and HO_2) in the MLT. Middle atmosphere water has been increasing in part due to the increase in CH_4 although there are also trends in the water entering from the troposphere to the stratosphere over the past several decades (Fujiwara et al. 2010). Trends in HOx have an important impact on mesospheric ozone, which is important for the radiative balance in the MLT (both as an absorber of solar ultraviolet radiation and as a component in chemical heating). Marsh et al. (2003) showed the response of ozone to trends in water in the mesosphere.

Another potential source of trends in MLT dynamics is from the waves that drive the circulation. There are several reasons to expect that the sources of gravity waves could

change as the Earth's climate changes. An important forcing is by tropical convection in the troposphere. As the thermal structure in the troposphere changes, the forcing of these waves will change as well. Becker (2009) used a gravity wave-resolving model to look at the differences with two different radiative forcings designed to represent the warming of the troposphere due to greenhouse gases. No differences were imposed on any other part of the model. The results of the Becker (2009) simulations showed an increase in gravity wave activity with the climate warming.

There is contradictory information about possible trends in MLT gravity waves. Offermann et al. (2011b) used standard deviation of temperature derived from nighttime airglow emitted at about 87 km as a proxy for gravity wave activity. They found an average seasonal cycle that fit with expectations from WACCM and they also found long-term variations. The long-term variations show different trends at the two different sites and were different for subsets of the 15-year analysis period; it is therefore not evident that there is any connection to long-term climate change. Hoffmann et al. (2011) showed observations of trends in gravity wave activity over a midlatitude site. The gravity wave activity changes were consistent with filtering by changing average winds in the mesosphere. As discussed in Sect. 4.1, filtering is a first-order process controlling the gravity waves that reach the MLT. Unfortunately, with the measurements available today, it is not possible to determine definitively to what extent observed changes in gravity waves are due to filtering by middle atmosphere winds and to what extent changing sources or other changes in local conditions contribute.

Jacobi et al. (2012) and Keuer et al. (2007) also reported on NH midlatitude MLT wind trends. Jacobi et al. (2012) noted the differences in the trends between North America and Europe, suggesting that changes in planetary waves contributed to the trends.

Trends in tidal sources can also occur, due either to tropospheric warming or to stratospheric ozone changes. Tides are excited in part by latent heat release in tropical convection and also have major sources from the solar radiation absorbed by tropospheric water vapor and stratospheric ozone. If the atmosphere warms while the relative humidity stays constant, the column will contain more water, which would imply a stronger tidal source in the troposphere. Stratospheric ozone decrease (and predicted recovery in upcoming decades) due to anthropogenic chlorine and bromine could affect tidal forcing in the stratosphere. In addition, the ozone heating has a solar cycle variation of several percent due to higher ozone and higher ultraviolet flux during solar maximum conditions.

A recent paper by Beig (2011a) summarizes the observations of trends in the MLT. The reported trends in temperature from different regions and different types of instrumentation still are not in agreement. For a global picture, Beig (2011a) emphasizes the trends derived from HALOE satellite observations by Remsberg (2007, 2009), Remsberg et al. (2008). Those observations indicate very weak cooling in the MLT region. However, the duration of the measurements is not long so the uncertainty in the magnitude and structure of the trends is high.

A long-time record that is sometimes used for trends is the frequency of polar mesospheric clouds, PMCs (e.g., Qian et al. 2011). This is particularly true in the NH, where observations go back to the nineteenth century. However, while the presence of PMCs depends sensitively on temperature, it also depends on water vapor content and possibly also on the distribution of cloud condensation nuclei. Therefore, efforts to deduce a temperature trend from these data encounter many uncertainties.

Simulations with global models are important in predicting the magnitude and vertical structure of trends. Because of the highly interactive nature of the energetics of the MLT, such simulations should include interactive chemistry and energetics, even if the goal is to

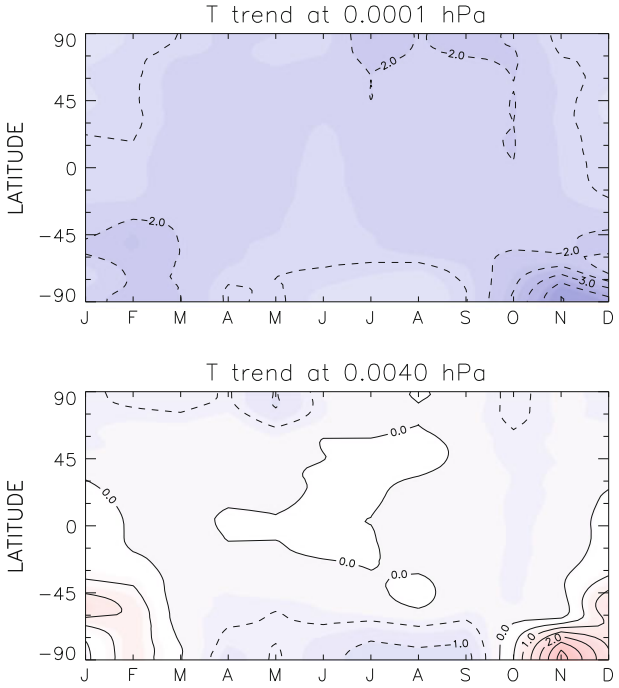

Fig. 17 Temperature trend simulated by WACCM for the period 1960–2005 as a function of month and latitude. *Top panel* is for 0.0003 hPa and *bottom panel* is for 0.004 hPa. Contour interval is 0.5 K/decade

describe the dynamical trends. Garcia et al. (2007) present WACCM simulations of the temperature trend over the period 1950–2003. These simulations include observed sea surface temperature and observed changes in anthropogenic gases and solar flux. The magnitude of the trend in temperature is at a local minimum in the MLT; it is negative with a magnitude of less than 0.5 K/decade. In a study using a mechanistic middle atmosphere, Berger and Lübken (2011) perform several simulations to determine what factors are most important in the trends. They note the importance of ozone loss in the stratosphere and its impact on the temperature. Unfortunately, comparisons of trends between models is difficult because of the different vertical grids: Berger and Lübken (2011) show most of their results on an altitude scale while Garcia et al. (2007) use pressure.

Predicted trends can have distinct seasonal variations. In WACCM, the largest trend in the MLT is in the high southern latitudes during November and December. Sect. 5.2 discusses the trend during this season and its association with dynamical changes in the stratosphere in response to the seasonal ozone hole in the lower stratosphere over Antarctica. The mechanism that forces this trend is confined to late spring and early summer in the SH. The restricted latitudinal and seasonal range of the strong trend is illustrated in Fig. 17, which shows the temperature trends for each month and latitude at two pressure levels. At 0.004 hPa, near the location of the summer mesopause, the trend is substantial near the South Pole. The analysis indicates that trends at this level can be either positive or negative; the trend at the South Pole in late spring is positive. At a higher level near the position of the tropical and winter mesopause (0.0001 hPa), the simulated temperature trend is negative during all months and at all latitudes. The strongest magnitudes are negative trends during November at the South Pole. As discussed by Smith et al. (2010b),

the temperature responses at both altitude regions are associated with changes in the gravity wave propagation due to filtering in the middle atmosphere.

7.2 Variations due to Solar and Charged Particle Forcing

The MLT responds to variations in the solar flux and to variations in energetic particle precipitation into the region. Heating in the MLT can also be affected indirectly by the transport of gases from the thermosphere. Both of these forcing processes vary on long timescales, including the approximate 11-year period of the sunspot cycle. The solar flux in the Schumann-Runge bands and Schumann-Runge continuum varies in phase with the solar cycle. The differences between solar minimum and solar maximum include changes in the temperature, the atmospheric density structure, and the composition.

The flux of energetic particles is intermittent but is more likely to occur when the Sun is active. Events are more common at solar maximum and in the declining phase of the solar cycle. The companion papers by Feofilov and Kutepov (2012) and Sinnhuber (2012) discuss these in more detail.

The mean dynamical response to solar flux variations are coupled with the photochemistry (Marsh et al. 2007). If there were no changes in composition, an increase in flux would lead to additional heating, increasing the mean temperature and the amplitude of the diurnally varying heating rate. Observations of the MLT response to the solar cycle summarized by Beig et al. (2003, 2008) and Beig (2011b) do show that the temperature is higher during periods of high solar activity although the magnitude of the warming differs in different analyses.

As is the case for the response of the atmosphere to anthropogenic gases, models provide guidance about the response of the MLT to solar variability. Model studies by Marsh et al. (2007) and Schmidt et al. (2006) emphasize the interactive chemistry and its contribution to the net trend in temperature. One of the important radiative gases is ozone, which itself has a marked solar cycle response due to the changes in both production and loss rates. The ozone production (a byproduct of O_2 photolysis) is positively correlated with the solar ultraviolet flux. The ozone loss rates in the mesosphere due to photolysis and catalytic reactions involving HOx molecules are also positively correlated with the solar ultraviolet flux. As a result, ozone itself can have either a positive or negative correlation, depending on details of the chemistry.

The relative magnitude of the variability of the solar flux varies with the energy in the solar spectrum. The timing also varies; i.e. the timing of the maximum flux shifts with the wavenumber of the radiation. Empirical models relating the variability in each wavenumber interval to an easily observed parameter such as the 10.7-cm flux (with a long record of daily ground-based observations) provide input fields needed for investigating the atmospheric response. Data to put together such models come from spectrally resolved observations from satellite.

The model described by Lean et al. (1997) and Lean (2000) has been used in a number of middle atmosphere models; see for example Eyring et al. (2006). The importance of the model, in particular the spectral makeup of the solar cycle variability, has been the focus of much discussion recently because of new observations from the Spectral Irradiance Monitor (SIM) on the SORCE satellite. SIM solar fluxes for the years 2004–2007 indicate that the solar variability for wavenumbers >200 nm is different than that in the Lean (2000) model (Harder et al. 2009; Fontenla et al. 2011). In particular, during solar maximum conditions the solar flux at 200–400 nm is substantially higher while that at wavenumbers >400 nm has the opposite sign (lower solar flux during solar maximum).

Numerical model studies using solar variability based on the SIM data by Haigh et al. (2010) and Merkel et al. (2011) focussed on the simulation of the solar cycle response of ozone in the stratosphere and lower mesosphere. In both cases, the models indicated expanded altitude ranges where the ozone response was negative (i.e., lower ozone concentrations for higher solar activity). Observational analysis of ozone measures by the Microwave Limb Sounder (MLS) (Haigh et al. 2010) and SABER (Merkel et al. 2011) agreed in some ways and disagreed in others with the simulations using SIM solar variability. Future work to extend the SIM model over a full solar cycle is needed to fully address this question. The response of temperature in the MLT was not presented in the model studies that have been published as of this writing.

8 Summary

Understanding of the dynamics of the MLT region continues to evolve as new measurements and analysis techniques are developed and numerical models include better representations of physical processes. This review paper describes an overview of the basic state and processes involved in large-scale dynamics. The review describes some of the developments in past decade.

A personal assessment of the key recent advances are listed here.

- The development of several comprehensive whole atmosphere numerical models allows for the investigation of interactions of the MLT with the troposphere and stratosphere below and the thermosphere above, as well as interactions between dynamics and chemistry.
- There is now recognition of the importance of nonmigrating tides. The new recognition is based on new observations that have enabled a more complete characterization of the global structure of these tidal modes.
- Evidence for connections in tides and mean temperatures between the winter stratosphere and the summer MLT is evidence of global coupling. There are still uncertainties but it appears that the mechanism for the coupling involves wave propagation, background wind and temperature changes, and the large-scale circulation.
- The recent publication of new data for the variations of spectrally resolved solar flux with the 11-year solar cycle raises questions about the solar cycle and the atmospheric response.
- Observations of temperature and trace species perturbations during active periods in NH winter have shown strong transport and changes in the mesosphere that had not been previously seen. Characterization of the dynamics and transport during these periods has led to the better understanding of the vertical coupling in the polar winter middle atmosphere.

Two long-lived (ongoing) satellites, TIMED and Envisat, have provided global data of the middle atmosphere for better characterization of climatology, interannual variability, and the interactions of dynamics with chemistry. This has been particularly valuable in the past decade because of highly active and variable dynamics in the NH winter middle atmosphere. The existing network of ground-based measurement systems has also increased; the combination of global satellite observations and detailed but localized ground-based data has been exploited in some investigations but holds the potential for further application to characterize and understand coupling across horizontal scales.

Future advances in understanding the MLT will be much reduced if there is an end to, or a gap in, observations by satellite that span the MLT region. This is a major threat to progress that cannot be compensated for by enhanced ground-based observing capabilities and state-of-the-art numerical models.

Acknowledgments The National Center for Atmospheric Research is sponsored by the National Science Foundation. This paper benefited from helpful comments by E. Becker, R. R. Garcia, and V. Yudin.

References

Achatz U, Grieger N, Schmidt H (2008) Mechanisms controlling the diurnal solar tide: analysis using a GCM and a linear model. J Geophys Res 113:A08303. doi:10.1029/2007JA012967

Akmaev RA (2001a) Seasonal variations of the terdiurnal tide in the mesosphere and lower thermosphere: a model study. Geophys Res Lett 28:3817–3820. doi:10.1029/2001GL013002

Akmaev RA (2001b) Simulation of large-scale dynamics in the mesosphere and lower thermosphere with the Doppler-spread parameterization of gravity waves. I, implementation and zonal mean climatologies. J Geophys Res 106:1193–1204

Akmaev RA (2007) On the energetics of mean-flow interactions with thermally dissipating gravity waves. J Geophys Res 112:D11125. doi:10.1029/2006JD007908

Akmaev RA (2011) Whole atmosphere modeling: connecting terrestrial and space weather. Rev Geophys 49:RG4004. doi:10.1029/2011RG000364

Akmaev RA, Fomichev VI (1998) Cooling of the mesosphere and lower thermosphere due to doubling of CO_2. Ann Geophys 16:1501–1512

Akmaev RA, Fuller-Rowell TJ, Wu F, Forbes JM, Zhang X, Anghel AF, Iredell MD, Moorthi S, Juang HM (2008) Tidal variability in the lower thermosphere: comparison of whole atmosphere model (WAM) simulations with observations from TIMED. Geophys Res Lett 86:L03810. doi:10.1029/2007GL032584

Alexander MJ, Barnet C (2007) Using satellite observations to constrain parameterizations of gravity wave effects for global models. J Atmos Sci 64:1652–1665

Alexander MJ, Dunkerton TJ (1999) A spectral parameterization of mean-flow forcing due to breaking gravity waves. J Atmos Sci 56:4167–4182

Andrews DG, McIntyre ME (1976) Planetary waves in horizontal and vertical shear: the generalized Eliassen-Palm relation and mean zonal acceleration. J Atmos Sci 33:2031–2048

Andrews DG, Holton JR, Leovy CB (1987) Middle atmosphere dynamics. Academic Press, San Diego

Angelats i Coll M, Forbes JM (2002) Nonlinear interactions in the upper atmosphere: the s = 1 and s = 3 nonmigrating semidiurnal tides. J Geophys Res 107:1157. doi:10.1029/2001JA900179

Aso T (2007) A note on the semidiurnal non-migrating tide at polar latitudes. Earth Planets Space 59:21–24

Baumgaertner AJG, McDonald AJ, Fraser GJ, Plank G (2005) Long-term observations of mean winds and tides in the upper mesosphere and lower thermosphere above Scott Base, Antarctica. J Atmos Solar Terr Phys 67:1480–1496

Baumgaertner AJG, Jarvis MJ, McDonald AJ, Fraser GJ (2006) Observations of the wavenumber 1 and 2 components of the semi-diurnal tide over Antarctica. J Atmos Solar Terr Phys 68:1195–1214

Baumgarten G (2010) Doppler Rayleigh/Mie/Raman lidar for wind and temperature measurements in the middle atmosphere up to 80 km. Atmos Meas Tech 3:1509–1518. doi:10.5194/amt-3-1509-2010

Beagley SR, Boone CD, Fomichev VI, Jin JJ, Semeniuk K, Mc Connell JC, Bernath PF (2010) First multi-year occultation observations of CO_2 in the MLT by ACE satellite: observations and analysis using the extended CMAM. Atmos Chem Phys 10:1133–1153

Becker E (2004) Direct heating rates associated with gravity wave saturation. J Atmos Solar Terr Phys 66:683–696

Becker E (2009) Sensitivity of the upper mesosphere to the Lorenz energy cycle of the troposphere. J Atmos Sci 66:647–666

Becker E (2011) Dynamical control of the middle atmosphere. Space Sci Rev (Online First) doi:10.1007/s11214-011-9841-5

Becker E, Fritts DC (2006) Enhanced gravity-wave activity and interhemispheric coupling during the MaCWAVE/MIDAS northern summer program 2002. Ann Geophys 60:103–118

Becker E, McLandress C (2009) Consistent scale interaction of gravity waves in the Doppler spread parameterization. J Atmos Sci 66:1434–1449

Becker E, Müllemann A, Lübken FJ, Körnich H, Hoffmann P, Rapp M (2004) High Rossby-wave activity in austral winter 2002: modulation of the general circulation of the MLT during the MaCWAVE/MIDAS northern summer program. Geophys Res Lett 31:L24S03. doi:10.1029/2004GL019615

Beig G (2011a) Long-term trends in the temperature of the mesosphere/lower thermosphere region: 1. Anthropogenic influences. J Geophys Res 116:A00H11. doi:10.1029/2011JA016646

Beig G (2011b) Long-term trends in the temperature of the mesosphere/lower thermosphere region: 2. Solar response. J Geophys Res 116:A00H12. doi:10.1029/2011JA016766

Beig G, Keckhut P, Lowe R, Roble R, Mlynczak M, Scheer J, Fomichev V, Offermann D, French W, Shepherd M, Semenov A, Remsberg E, She C, Lubken F, Bremer J, Clemesha B, Stegman J, Sigernes F, Fadnavis S (2003) Review of mesospheric temperature trends. Rev Geophys 41:1015. doi:10.1029/2002RG000121

Beig G, Scheer J, Mlynczak MG, Keckhut P (2008) Overview of the temperature response in the mesosphere and lower thermosphere to solar activity. Rev Geophys 46:RG3002. doi:10.1029/2007RG000236

Berger U, Lübken FJ (2011) Mesospheric temperature trends at midlatitudes in summer. Geophys Res Lett 38:L22804. doi:10.1029/2011GL049528

Bishop RL, Larsen MF, Hecht JH, Liu AZ, Gardner CS (2004) Mesospheric and lower thermospheric diffusivities and instability layers. J Geophys Res 109:D02S03. doi:10.1029/2002JD00307

Bittner M, Offermann D, Graef HH, Donner M, Hamilton K (2002) An 18-year time series of OH rotational temperatures and middle atmosphere decadal variations. J Atmos Solar Terr Phys 64(8–11):1147–1166. doi:10.1016/S1364-6826(02)00065-2

Bremer J, Peters D (2008) Influence of stratospheric ozone changes on longterm trends in the meso- and lower-thermosphere. J Atmos Solar Terr Phys 70:1473–1481

Burrage MD, Skinner WR, Marshall AR, Hays PB, Lieberman RS, Franke SJ, Gell DA, Ortland DA, Morton YT, Schmidlin FJ, Vincent RA, Wu DL (1993) Comparison of HRDI wind measurements with radar and rocket observations. Geophys Res Lett 20:1259–1263

Burrage MD, Wu DL, Skinner WR, Ortland DA, Hays PB (1995) Latitude and seasonal dependence of the semidiurnal tide observed by the high-resolution Doppler imager. J Geophys Res 100:11,313–11,321

Chandran A, Rusch DW, Merkel AW, Palo SE, Thomas GE, Taylor MJ, Bailey SM, Russell JM III (2010) Polar mesospheric cloud structures observed from the cloud imaging and particle size experiment on the aeronomy of ice in the mesosphere spacecraft: atmospheric gravity waves as drivers for longitudinal variability in polar mesospheric cloud occurrence. J Geophys Res 38:D13102. doi:10.1029/2009JD013185

Chandran A, Collins RL, Garcia RR, Marsh DR (2011) A case study of an elevated stratopause generated in the whole atmosphere community climate model. Geophys Res Lett 38:L08804. doi:10.1029/2010GL046566

Chang LC, Palo SE, Liu HL (2009) Short-term variation of the s = 1 nonmigrating semidiurnal tide during the 2002 stratospheric sudden warming. J Geophys Res 114:D03109. doi:10.1029/2008JD010886

Chang LC, Palo SE, Liu HL, Fang TW, Lin CS (2010) Response of the thermosphere and ionosphere to an ultra fast Kelvin wave. J Geophys Res 115:A00G04. doi:10.1029/2010JA015453

Chang LC, Palo SE, Liu HL (2011) Short-term variability in the migrating diurnal tide caused by interactions with the quasi 2 day wavee. J Geophys Res 116:D12112. doi:10.1029/2010JD014996

Chapman S, Lindzen RS (1970) Atmospheric tides. Gordon and Breach, New York

Charlton AJ, Polvani LM (2007) A new look at stratospheric sudden warmings, part I: climatology and modeling benchmarks. J Clim 20:449–469

Charney JG, Drazin PG (1961) Propagation of planetary-scale disturbances from the lower into the upper atmosphere. J Geophys Res 66:83–109

Chu X (2003) Lidar studies of interannual, seasonal, and diurnal variations of polar mesospheric clouds at the South Pole. J Geophys Res 108:8447. doi:10.1029/2002JD002524

Chu X, Espy PJ, Nott GJ, Diettrich JC, Gardner CS (2006) Polar mesospheric clouds observed by an iron Boltzmann lidar at Rothera (67.5°S, 68.0°W), Antarctica from 2002 to 2005: properties and implications. J Geophys Res 111:D20213. doi:10.1029/2006JD007086

Coy L, Fritts DC (1988) Gravity wave heat fluxes: a Lagrangian approach. J Atmos Sci 45:1770–1780

Day KA, Mitchell NJ (2010) The 16-day wave in the Arctic and Antarctic mesosphere and lower thermosphere. Atmos Chem Phys 10:1461–1472

Dickinson RE (1968) Planetary rossby waves propagating vertically through weak westerly wind wave guides. J Atmos Sci 25:984–1002

Dowdy A, Vincent RA, Igarashi K, Murayama Y, Murphy DJ (2001) A comparison of mean winds and gravity wave activity in the northern and southern polar MLT. Geophys Res Lett 28:1475–1478

Dowdy AJ, Vincent RA, Tsutsumi M, Igarashi K, Murayama Y, Singer W, Murphy DJ (2007) Polar mesosphere and lower thermosphere dynamics: 1. Mean wind and gravity wave climatologies. J Geophys Res 112:D17104. doi:10.1029/2006JD008126

Drob DP, Emmert JT, Crowley G, Picone JM, Shepherd GG, Skinner W, Hays P, Niciejewski RJ, Larsen M, She CY, Meriwether JW, Hernandez G, Jarvis MJ, Sipler DP, Tepley CA, OBrien MS, Bowman JR, Wu Q, Murayama Y, Kawamura S, Reid IM, Vincent RA (2008) An empirical model of the earths horizontal wind fields: HWM07. J Geophys Res 113:A12304. doi:10.1029/2008JA013668

Du J, Ward WE (2005) Terdiurnal tide in the extended Canadian middle atmospheric model (CMAM). Geophys Res Lett 115:D24106. doi:10.1029/2010JD014479

Dunkerton TJ (1978) On the mean meridional mass motions of the stratosphere and mesosphere. J Atmos Sci 35:2325–2333

Dunkerton TJ (1982) Theory of the mesopause semiannual oscillation. J Atmos Sci 39:2681–2690

Ejiri MK, Taylor MJ, Nakamura T, Franke SJ (2009) Critical level interaction of a gravity wave with background winds driven by a large-scale wave perturbation. J Geophys Res 114(114):D18117. doi:10.1029/2008JD011381

Emmert JT, Drob DP, Shepherd GG, Hernandez G, Jarvis MJ, Meriwether JW, Niciejewski RJ, Sipler DP, Tepley CA (2008) DWM07 global empirical model of upper thermospheric storm-induced disturbance windss. J Geophys Res 113:A11319. doi:10.1029/2008JA013541

Ern M, Preusse P, Gille JC, Hepplewhite CL, Mlynczak MG, Russell JM III, Riese M (2011) Implications for atmospheric dynamics derived from global observations of gravity wave momentum flux in stratosphere and mesosphere. J Geophys Res 116:D19107. doi:10.1029/2011JD015821

Espy PJ, Fernandez SO, Forkman P, Murtagh D, Stegman J (2011) The role of the QBO in the inter-hemispheric coupling of summer mesospheric temperatures. Atmos Chem Phys 11:495–502. doi:10.5194/acp-11-495-2011

Eyring V, Butchart N, Waugh DW, Akiyoshi H, Austin J, Bekki S, Bodeker GE, Boville BA, Brühl C, Chipperfield MP, Cordero E, Dameris M, Deushi M, Fioletov VE, Frith SM, Garcia RR, Gettelman A, Giorgetta MA, Grewe V, Jourdain L, Kinnison DE, Mancini E, Manzini E, Marchand M, Marsh DR, Nagashima T, Nielsen E, Newman PA, Pawson S, Pitari G, Plummer DA, Rozanov E, Schraner M, Shepherd TG, Shibata K, Stolarski RS, Struthers H, Tian W, Yoshiki M (2006) Assessment of temperature, trace species and ozone in chemistry-climate simulations of the recent past. J Geophys Res 111(D22):D22308. doi:10.1029/2006JD007327

Eyring V, Shepherd TG, Waugh DW (eds) (2010) SPARC Report on the Evaluation of Chemistry-Climate Models. WCRP-132, WMO/TD-No.1526

Feofilov AG, Kutepov AA (2012) Infrared radiance in the mesosphere and lower thermosphere. Surv Geophys This issue

Fleming EL, Chandra S, Burrage MD, Skinner WR, Hays PB, Solheim BH, Shepherd GG (1996) Climatological mean wind observations from the UARS high-resolution Doppler imager and wind imaging interferometer: comparison with current reference models. J Geophys Res 101:10,455–10,473

Fomichev VI (2009) The radiative energy budget of the middle atmosphere and its parameterization in general circulation models. J Atmos Solar Terr Phys 71:1577–1585. doi:110.1016/j.jastp.2009.04.007

Fontenla JM, Harder J, Livingston W, Snow M, Woods T (2011) High-resolution solar spectral irradiance from extreme ultraviolet to far infrared. J Geophys Res 116:D20108. doi:10.1029/2011JD016032

Forbes JM, Hagan ME (1982) Thermospheric extensions of the classical expansion functions for semidiurnal tides. J Geophys Res 87:5253–5259

Forbes JM, Makarov NA, Portnyagin YI (1995) First results from the meteor radar at South Pole: a large 12-hour oscillation with zonal wavenumber one. Geophys Res Lett 22:3247–3250

Forbes JM, Zhang X, Ward W, Talaat ER (2002) Climatological features of mesosphere and lower thermosphere stationary planetary waves within ±40° latitude. J Geophys Res 107:4322. doi:10.1029/2001JD001232

Forbes JM, Zhang X, Palo SE, Russell J, Mertens CJ, Mlynczak M (2009) Kelvin waves in stratosphere, mesosphere and lower thermosphere temperatures as observed by TIMED/SABER during 2002–2006. Earth Planets Space 61:447–453

Franke SJ, Chu X, Liu AZ, Hocking WK (2005) Comparison of meteor radar and Na Doppler lidar measurements of winds in the mesopause region above Maui, Hawaii. J Geophys Res 110:D09S02. doi:10.1029/2003JD004486

French WJR, Klekociuk AR (2011) Long-term trends in Antarctic winter hydroxyl temperatures. J Geophys Res 116:D00P09. doi:10.1029/2011JD015731

French WJR, Mulligan FJ (2010) Stability of temperatures from TIMED/SABER v1.07 (2002–2009) and Aura/MLS v2.2 (2004–2009) compared with OH(6-2) temperatures observed at Davis Station, Antarctica. Atmos Chem Phys 10:11,439–11,446

Fritts DC, Alexander MJ (2003) Gravity wave dynamics and effects in the middle atmosphere. Rev Geophys 41:1003. doi:10.1029/2001RG000106
Fritts DC, Isler JR (1994) Mean motions and tidal and two-day wave structure and variability in the mesosphere and lower thermosphere over Hawaii. J Atmos Sci 51:2145–2164
Fujiwara M, Vomel H, Hasebe F, Ogino S-Y, Iwasaki S, Nishi N, Shibata T, Shimizu K, Nishimoto E, Valverde Canossa JM, Selkirk HB, Oltmans SJ (2010) Seasonal to decadal variations of water vapor in the tropical lower stratosphere observed with balloon-borne cryogenic frost point hygrometers. J Geophys Res 115:D18304. doi:10.1029/2010JD014179
Garcia RR, Dunkerton TJ, Lieberman RS, Vincent RA (1997) Climatology of the semiannual oscillation of the tropical middle atmosphere. J Geophys Res 102:26,019–26,032
Garcia RR, Lieberman R, Russell JM III, Mlynczak MG (2005) Large-scale waves in the mesosphere and lower thermosphere observed by SABER. J Atmos Sci 62:4384–4399
Garcia RR, Marsh DR, Kinnison DE, Boville BA, Sassi F (2007) Simulation of secular trends in the middle atmosphere, 1950–2003. J Geophys Res 112:D09301. doi:10.1029/2006JD007485
Grygalashvyly M, Becker E, Sonnemann G (2011) Gravitywave mixing and effective diffusivity for minor chemical constituents in the mesosphere/lower thermosphere. Space Sci Rev (Online First) doi:10.1007/s11214-011-9857-x
Gumbel J, Karlsson B (2011) Intra- and inter-hemispheric coupling effects on the polar summer mesosphere. Geophys Res Lett 38:L14804. doi:10.1029/2011GL047968
Hagan ME, Forbes JM (2002) Migrating and nonmigrating diurnal tides in the middle and upper atmosphere excited by tropospheric latent heat release. J Geophys Res 107:4754. doi:10.1029/2001JD001236
Hagan ME, Maute A, Roble RG (2009) Tropospheric tidal effects on the middle and upper atmosphere. J Geophys Res 114:A01302. doi:10.1029/2008JA0136376
Haigh JD, Roscoe HK (2009) The final warming date of the Antarctic polar vortex and influences on its interannual variability. J Clim 22:5809–5819. doi:10.1175/2009JCLI2865
Haigh JD, Winning AR, Toumi R, Harder JW (2010) An influence of solar spectral variations on radiative forcing of climate. Nature 467:696–699. doi:10.1038/nature09426
Hall CM, Hoppe UP (1998) Estimates of turbulent energy dissipation rates from determinations of characteristic vertical wavenumber by EISCAT. Geophys Res Lett 25:4075–4078
Harder JW, Fontenla JM, Pilewskie P, Richard EC, Woods TN (2009) Trends in solar spectral irradiance variability in the visible and infrared. Geophys Res Lett 36:L07801. doi:10.1029/2008GL036797
Hecht JH (2004) Instability layers and airglow imaging. Rev Geophys 42:RG1001. doi:10.1029/2003RG000131
Hedin AE (1991) Extension of the MSIS thermospheric model into the middle and lower atmosphere. J Geophys Res 96:1159
Hernandez G (2004) Winter mesospheric temperatures above South pole (90°S) and their relationship to the springtime ozone hole size. Geophys Res Lett 31:L07109. doi:10.1029/2004GL019414
Hervig M, Siskind D (2006) Decadal and inter-hemispheric variability in polar mesospheric clouds, water vapor, and temperature. J Atmos Solar Terr Phys 68:30–41
Hibbins RE, Marsh OJ, McDonald AJ, Jarvis MJ (2010) A new perspective on the longitudinal variability of the semidiurnal tide. Geophys Res Lett 37:L14804. doi:10.1029/2010GL044015
Hines CO (1997a) Doppler-spread parameterization of gravity-wave momentum deposition in the middle atmosphere, 1, basic formulation. J Atmos Solar Terr Phys 59:371–386
Hines CO (1997b) Doppler-spread parameterization of gravity-wave momentum deposition in the middle atmosphere, 2, broad and quasi monochromatic spectra, and implementation. J Atmos Solar Terr Phys 59:387–400
Hoffmann P, Singer W, Keuer D, Hocking W, Kunze M, Murayama Y (2007) Latitudinal and longitudinal variability of mesospheric winds and temperatures during stratospheric warming events. J Atmos Solar Terr Phys 69:2355–2366
Hoffmann P, Rapp M, Singer W, Keuer D (2011) Trends of mesospheric gravity waves at northern middle latitudes during summer. J Geophys Res 116:D00P08. doi:10.1029/2011JD015717
Holton JR (1983) The influence of gravity wave breaking on the general circulation of the middle atmosphere. J Atmos Sci 40:2497–2507
Huaman MM, Balsley BB (1999) Differences in near-mesopause summer winds, temperatures, and water vapor at northern and southern latitudes as possible causal factors in inter-hemispheric PMSE differences. Geophys Res Lett 26:1529–1532
Huang FT, Reber CA (2003) Seasonal behavior of the semidiurnal and diurnal tides, and mean flows at 95 km, based on measurements from the High Resolution Doppler Imager (HRDI) on the Upper Atmosphere Research Satellite (UARS). J Geophys Res 108:4360. doi:10.1029/2002JD003189

Huang FT, Mayr HG, Reber CA, Russell JM, Mlynczak M, Mengel JG (2006) Stratospheric and mesospheric temperature variations for the quasi-biennial and semiannual (QBO and SAO) oscillations based on measurements from SABER (TIMED) and MLS (UARS). Ann Geophys 24:2131–2149

Iimura H, Palo SE, Wu Q, Killeen TL, Solomon SC, Skinner WR (2009) Structure of the nonmigrating semidiurnal tide above Antarctica observed from the TIMED Doppler Interferometer. J Geophys Res 114:D11102. doi:10.1029/2008JD010608

Jacobi C, Hoffmann P, Liu R, Merzlyakov E, Portnyagin Y, Manson A, Meek C (2012) Long-term trends, their changes, and interannual variability of northern hemisphere midlatitude MLT windsl. J Atmos Solar Terr Phys 75–76:81–89. doi:10.1016/j.jastp.2011.03.016

Karlsson B, Kornich H, Gumbel J (2007) Evidence for interhemispheric stratosphere-mesosphere coupling derived from noctilucent cloud properties. Geophys Res Lett 34:L16806. doi:10.1029/2007GL030282

Karlsson B, Mc Landress C, Shepherd TG (2009) Inter-hemispheric mesospheric coupling in a comprehensive middle atmosphere model. J Atmos Solar Terr Phys 71:518–530

Karlsson B, Randall CE, Benze S, Mills M, Harvey VL, Bailey SM, Russell JM III (2009) Intra-seasonal variability of polar mesospheric clouds due to inter-hemispheric coupling. Geophys Res Lett 36:L20802. doi:10.1029/2009GL040348

Karpetchko A, Kyrö E, Knudsen BM (2005) Arctic and Antarctic polar vortices 1957–2002 as seen from the ERA-40 reanalyses. J Geophys Res 110(D21):D21109. doi:10.1029/2005JD006113

Kelley MC, Kruschwitz CA, Gardner CS, Drummond JD, Kane TJ (2003) Mesospheric turbulence measurements from persistent Leonid meteor train observations. J Geophys Res 108:8454. doi:10.1029/2002JD002392

Keuer D, Hoffmann P, Singer W, Bremer J (2007) Long-term variations of the mesospheric wind field at mid-latitude. Ann Geophys 25:1779–1790

Kim YJ, Eckermann SD, Chun H (2003) An overview of the past, present and future of gravity-wave drag parametrization for numerical climate and weather prediction models. Atmos Ocean 41:65–98

Kirkwood S, Nilsson H, Morris RJ, Klekociuk AR, Holdsworth DA, Mitchell NJ (2008) A new height for the summer mesopause: Antarctica, December 2007. Geophys Res Lett 35:L23810. doi:10.1029/2008GL035915

Kornich H, Becker E (2010) A simple model for the interhemispheric coupling of the middle atmosphere circulation. Adv Space Res 45:661–668

Kvissel OK, Orsolini YJ, Stordal F, Limpasuvan V, Richter J, Marsh DR (2012) Mesospheric intrusion and anomalous chemistry during and after a major stratospheric sudden warming. J Atmos Solar Terr Phys 78–79:116–124. doi:10.1016/j.jastp.2011.08.015

Lean JL (2000) Evolution of the Suns spectral irradiance since the Maunder Minimum. Geophys Res Lett 27:2425–2428. doi:10.1029/2000GL000043

Lean JL, Rottman GJ, Kyle HL, Woods TN, Hickey JR, Puga LC (1997) Detection and parameterization of variations in solar midand near-ultraviolet radiation (200–400 nm). J Geophys Res 102:29939–29956

Leovy CB (1964) Simple models of thermally driven mesospheric circulation. J Atmos Sci 21:327–341

Lieberman RS (1993) Long-term variations of zonal mean winds and (1,1) driving in the equatorial lower thermosphere. J Atmos Solar Terr Phys 59:1483–1490

Lieberman RS, Burrage MD, Gell DA, Hays PB, Marshall AR, Ortland DA, Skinner WR, Wu DL, Vincent RA, Franke SJ (1993) Zonal mean winds in the equatorial mesosphere and lower thermosphere observed by the High Resolution Doppler Imager. Geophys Res Lett 20:2849–2852

Lieberman RS, Smith AK, Franke SJ, Vincent RA, Isler JR, Manson AH, Meek CE, Fraser GJ, Fahrutdinova A, Thayaparan T, Hocking W, MacDougall J, Nakamura T, Tsuda T (2000) Comparison of mesospheric and lower thermospheric residual wind with High Resolution Doppler Imager, medium frequency, and meteor radar winds. J Geophys Res 105:27,023–27,035

Lieberman RS, Ortland DA, Yarosh ES (2003) Climatology and interannual variability of diurnal water vapor heating. J Geophys Res 108:4123. doi:10.1029/2002JD002308

Lieberman RS, Oberheide J, Hagan ME, Remsberg EE, Gordley LL (2004) Variability of diurnal tides and planetary waves during November 1978–May 1979. J Atmos Solar Terr Phys 65:517–528

Lieberman RS, Riggin DM, Ortland DA, Nesbitt SW, Vincent RA (2007) Variability of mesospheric diurnal tides and tropospheric diurnal heating during 1997–1998. J Geophys Res 112:D20110. doi:10.1029/2007JD008578

Lieberman RS, Ortland DA, Riggin DM, Wu Q, Jacobi C (2010) Momentum budget of the migrating diurnal tide in the mesosphere and lower thermosphere. J Geophys Res 115:D20105. doi:10.1029/2009JD013684

Limpasuvan V, Wu DL (2009) Anomalous two day wave behavior during the 2006 austral summer. Geophys Res Lett 36:L04807. doi:10.1029/2008GL036387

Limpasuvan V, Richter JH, Orsolini YJ, Stordal F, Kvissel O (2011) The roles of planetary and gravity waves during a major stratospheric sudden warming as characterized in WACCM. J Atmos Solar Terr Phys 73. doi:10.1016/j.jastp.2011.03.004

Lindzen RS (1981) Turbulence and stress owing to gravity wave and tidal breakdown. J Geophys Res 86:9707–9714

Liu AZ (2009) Estimate eddy diffusion coefficients from gravity wave vertical momentum and heat fluxes. Geophys Res Lett 36:L08806

Liu HL (2000) Temperature changes due to gravity wave saturation. J Geophys Res 105:12,329–12,336

Liu HL, Roble RG (2002) A study of a self-generated stratospheric sudden warming and its mesospheric-lower thermospheric impacts using the coupled TIME-GCM/CCM3. J Geophys Res 107:4695. doi:10.1029/2001JD001533

Liu HL, Hays PB, Roble RG (1999) A numerical study of gravity wave breaking and impacts on turbulence and mean state. J Atmos Sci 56:2152–2177

Liu HL, Talaat ER, Roble RG, Lieberman RS, Riggin DM, Yee JH (2004) The 6.5-day wave and its seasonal variability in the middle and upper atmosphere. J Geophys Res 109:D211125. doi:10.1029/2004JD004795

Liu HL, Li T, She CY, Oberheide J, Wu Q, Hagan ME, Xu J, Roble RG, Mlynczak MG, Russell JM III (2007) Comparative study of short-term diurnal tidal variability. J Geophys Res 112:D18108. doi:10.1029/2007JD008542

Liu HL, Sassi F, Garcia RR (2009) Error growth in a whole atmosphere climate model. J Atmos Sci 66:173–186. doi:10.1175/2008JAS2825.1

Liu HL, Foster BT, Hagan ME, McInerney JM, Maute A, Qian L, Richmond AD, Roble RG, Solomon SC, Garcia RR, Kinnison D, Marsh DR, Smith AK, Richter J, Sassi F, Oberheide J (2010) Thermosphere extension of the whole atmosphere community climate model. J Geophys Res 115:A12302. doi:10.1029/2010JA015586

López Puertas M, López Valverde MA, Garcia RR, Roble RG (2000) A review of CO_2 and CO abundances in the middle atmosphere. In: Siskind DE, Eckermann SD, Summers ME (eds) Atmospheric science across the stratopause. AGU, Washington, D. C., pp 83–100

Lossow S, McLandress C, Jonsson AI, Shepherd TG (2012) Influence of the Antarctic ozone hole on the polar mesopause region as simulated by the Canadian middle atmosphere model. J Atmos Solar Terr Phys 74:111–123

Lübken F (1997) Seasonal variation of turbulent energy dissipation rates at high latitudes as determined by in situ measurements of neutral density fluctuations. J Geophys Res 102:13,441–13,456

Lübken F, Höffner J, Viehl TP, Kaifler B, Morris RJ (2011) First measurements of thermal tides in the summer mesopause region at Antarctic latitudes. Geophys Res Lett 38:L24806. doi:10.1029/2011GL0500458

Manney GL, Krüger K, Sabutis JL, Amina Sena S, Pawson S (2005) The remarkable 2003–2004 winter and other recent warm winters in the Arctic stratosphere in the late 1990s. J Geophys Res 110:D04107. doi:10.1029/2004JD005367

Manney GL, Krüger K, Pawson S, Minschwaner K, Schwartz MJ, Daffer WH, Livesey NJ, Mlynczak MG, Remsberg EE, Russell JM III, Waters JW (2008) The evolution of the stratopause during the 2006 major warming: satellite data and assimilated meteorological analyses. J Geophys Res 113:D11115. doi:10.1029/2007JD009097

Manney GL, Schwartz MJ, Krüger K, Santee ML, Pawson S, Lee JN, Daffer WH, Fuller RA, Livesey NJ (2009) Aura Microwave Limb Sounder observations of dynamics and transport during the record-breaking 2009 Arctic stratospheric major warming. Geophys Res Lett 36:L12815. doi:10.1029/2009GL038586

Marsh D, Smith A, Noble E (2003) Mesospheric ozone response to changes in water vapor. J Geophys Res 108(D3):4109. doi:10.1029/2002JD002705

Marsh D, Garcia RR, Kinnison DE, Bouville BA, Sassi F, Solomon SC, Matthes K (2007) Modeling the whole atmosphere response to solar cycle changes in radiative and geomagnetic forcing. J Geophys Res 112:D23306. doi:10.1029/2006JD008306

Marsh DR (2011) Chemical-dynamical coupling in the mesosphere and lower thermosphere. In: Abdu M, Pancheva D, Bhattacharyya A (eds) Aeronomy of the Earth's atmosphere and ionosphere, IAGA Special Sopron Book Ser., vol 2. Springer, Dordrecht

Marsh DR, Russell JM (2000) A tidal explanation for the sunrise/sunset anomaly in HALOE low-latitude nitric oxide observations. Geophys Res Lett 27:3197–3200

Mayr HG, Mengel JG (2005) Interannual variations of the diurnal tide in the mesosphere generated by the quasi-biennial oscillation. J Geophys Res 110:D10111. doi:10.1029/2004JD005055

McLandress C (2002a) The seasonal variation of the propagating diurnal tide in the mesosphere and lower thermosphere. Part 1: the role of gravity waves and planetary waves. J Atmos Sci 59:893–906
McLandress C (2002b) The seasonal variation of the propagating diurnal tide in the mesosphere and lower thermosphere. Part 2: the role of tidal heating and mean winds. J Atmos Sci 59:907–922
McLandress C, Scinocca JF (2005) The GCM response to current parameterizations of nonorographic gravity wave drag. J Atmos Sci 62:2394–2413
McLandress C, Shepherd GG, Solheim BH, Burrage MD, Hays PB, Skinner WR (1996) Combined mesosphere/thermosphere winds using WINDII and HRDI data from the Upper Atmosphere Research Satellite. J Geophys Res 101:10,441–10,453
Medvedev AS, Klaasen GP (2000) Parameterization of gravity wave momentum deposition based on nonlinear wave interactions: basic formulation and sensitivity tests. J Atmos Solar Terr Phys 62:1015–1033
Medvedev AS, Klaasen GP (2003) Thermal effects of saturating gravity waves in the atmosphere. J Geophys Res 108:4040. doi:10.1029/2002JD002504
Merkel AW, Harder JW, Marsh DR, Smith AK, Fontenla JM, Woods TN (2011) The impact of solar spectral irradiance variability on middle atmospheric ozone. Geophys Res Lett 38:L13802. doi:10.1029/2011GL047561
Mitchell NJ, Pancheva D, Middleton HR, Hagan ME (2002) Mean winds and tides in the Arctic mesosphere and lower thermosphere. J Geophys Res 107:1004. doi:10.1029/2001JA900127
Mlynczak MG, Solomon S (1993) A detail evaluation of the heating efficiency in the middle atmosphere. J Geophys Res 98:10,517–10,541
Mukhtarov P, Pancheva D, Andonov B (2010) Climatology of the stationary planetary waves seen in the SABER/TIMED temperatures (2002–2007). J Geophys Res 115:A06315. doi:10.1029/2009JA015156
Murphy DJ, Tsutsumi M, Riggin DM, Jones GOL, Vincent RA, Hagan ME, Avery SK (2003) Observations of a nonmigrating component of the semidiurnal tide over Antarctica. J Geophys Res 108:4241. doi:10.1029/2002JD003077
Murphy DJ, Forbes JM, LWalterscheid R, Hagan ME, Avery SK, Aso T, Fraser GJ, Fritts DC, Jarvis MJ, McDonald AJ, Riggin DM, Tsutsumi M, Vincent RA (2006) A climatology of tides in the Antarctic mesosphere and lower thermosphere. J Geophys Res 111. doi:10.1029/2005JD006803
Murphy DJ, Aso T, Fritts DC, Hibbins RE, McDonald AJ, Riggin DM, Tsutsumi M, Vincent RA (2009) Source regions for Antarctic MLT non-migrating semidiurnal tides. Geophys Res Lett 36:L09805. doi:10.1029/2008GL037064
Niciejewski R, Skinner W, Cooper M, Marshall A (2011) Resolving dynamics structure in the MLT: correlative measurements with TIDI and HRDI. Abstract SA33A-07 presented at 2011 Fall meeting, AGU, San Francisco, California, 5–9 Dec
Oberheide J, Forbes JM (2008) Tidal propagation of deep tropical cloud signatures into the thermosphere from TIMED observations. Geophys Res Lett 35:L04816. doi:10.1029/2007GL032397
Oberheide J, Hagan ME, Roble RG, Offermann D (2002) Sources of nonmigrating tides in the tropical middle atmosphere. J Geophys Res 107:4567. doi:10.1029/2002JD002220
Oberheide J, Hagan ME, Roble RG (2003) Tidal signatures and aliasing in temperature data from slowly precessing satellites. J Geophys Res 108:1055. doi:10.1029/2002JA009585
Oberheide J, Wu Q, Ortland DA, Killeen TL, Hagan ME, Roble RG, Niciejewski RJ, Skinner W (2005) Non-migrating diurnal tides as measured by the TIMED Doppler interferometer: preliminary results. Adv Space Res 45:1911–1917
Oberheide J, Wu Q, Killeen TL, Hagan ME, Roble RG (2006) Diurnal nonmigrating tides from TIMED Doppler Interferometer wind data: monthly climatologies and seasonal variations. J Geophys Res 111:A10S03. doi:10.1029/2005JA011491
Offermann D, Jarisch M, Schmidt H, Oberheide J, Grossmann KU, Gusev O, Russell JM III, Mlynczak M (2007) The wave turbopause. J Atmos Solar Terr Phys 69:2139–2158
Offermann D, Hoffmann P, Knieling P, Koppmann R, Oberheide J, Riggin DM, Tunbridge VM, Steinbrecht W (2011) Quasi 2 day waves in the summer mesosphere: triple structure of amplitudes and long-term development. J Geophys Res 116:D00P02. doi:10.1029/2010JD015051
Offermann D, Wintel J, Kalicinsky C, Knieling P, Koppmann R, Steinbrecht W (2011) Long-term development of short-period gravity waves in middle Europe. J Geophys Res 116:D00P07. doi:10.1029/2010JD015544
Orsolini YJ, Urban J, Murtagh DP, Lossow S, Limpasuvan V (2010) Descent from the polar mesosphere and anomalously high stratopause observed in 8 years of water vapor and temperature satellite observations by the Odin Sub-Millimeter Radiometer. J Geophys Res 115:D12305. doi:10.1029/2009JD013501
Ortland DA (2005a) Generalized Hough modes: the structure of damped global-scale waves propagating on a mean flow with horizontal and vertical shear. J Atmos Sci 62:2674–2683

Ortland DA (2005b) A study of the global structure of the migrating diurnal tide using generalized Hough modes. J Atmos Sci 62:2684–2702

Ortland DA, Alexander MJ (2006) Gravity wave influence on the global structure of the diurnal tide in the mesosphere and lower thermosphere. J Geophys Res 111:A10S10. doi:10.1029/2005JA011467

Pancheva D, Merzlyakov E, Mitchell NJ, Portnyagin Y, Manson AH, Jacobi C, Meek CE, Luo Y, Clark RR, Hocking W, MacDougall J, Muller HG, Kurschner D, Jones GOL, Vincent RA, Reid IM, Singer W, Igarashi K, Fahrutdinova GIFNAN, Stepanov AM, Poole LMG, Malinga SB, Kashcheyev BL, Oleynikov AN (2002) Global-scale tidal structure in the mesosphere & lower thermosphere during the PSMOS campaign summer-99 and comparison with the global scale wave model. J Atmos Solar Terr Phys 64:1011–1035

Pancheva D, Mukhtarov P, Mitchell NJ, Merzlyakov E, Smith A, Andonov B, Singer W, Hocking W, Meek C, Manson A, Murayama Y (2008) Planetary waves in coupling the stratosphere and mesosphere during the major stratospheric warming in 2003/2004. J Geophys Res 113:D12105. doi:10.1029/2007JD009011

Pancheva D, Mukhtarov P, Andonov B (2009) Global structure, seasonal and interannual variability of the migrating semidiurnal tide seen in the SABER/TIMED temperatures (2002–2007). Ann Geophys 27:687–703

Pancheva D, Mukhtarov P, Andonov B, Mitchell NJ, Forbes JM (2009a) Planetary waves observed by TIMED/SABER in coupling the stratosphere–mesosphere–lower thermosphere during the winter of 2003/2004: part 1, Comparison with the ukmo temperature results. J Atmos Solar Terr Phys 71:61–74

Pancheva D, Mukhtarov P, Andonov B, Mitchell NJ, Forbes JM (2009b) Planetary waves observed by TIMED/SABER in coupling the stratosphere–mesosphere–lower thermosphere during the winter of 2003/2004: part 2, altitude and latitude planetary wave structure. J Atmos Solar Terr Phys 71:75–87

Picone JM, Hedin AE, Drob DP, Aiken AC (2002) NRLMSIS-00 empirical model of the atmosphere: statistical comparisons and scientific issues. J Geophys Res 107:1468. doi:10.1029/2002JA009430

Portnyagin YI, Forbes JM, Makarov NA, Merzlyakov EG, Palo S (1998) The summertime 12-hour wind oscillation with zonal wavenumber s = 1 in the lower thermosphere over the South Pole. Ann Geophys 16:828–837

Preusse P, Eckermann SD, Ern M, Oberheide J, Picard RH, Roble RG, Riese M, Russell JM III, Mlynczak MG (2009) Global ray tracing simulations of the SABER gravity wave climatology. J Geophys Res 113:D08126. doi:10.1029/2008JD011214

Qian L, Laštovička J, Roble RG, Solomon SC (2011) Progress in observations and simulations of global change in the upper atmosphere. J Geophys Res 116:A00H03. doi:10.1029/2010JA016317

Randall CE, Harvey VL, Singleton CS, Bernath PF, Boone CD, Walker KA (2009) NO_x descent in the Arctic middle atmosphere in early 2009. Geophys Res Lett 36:L18811. doi:10.1029/2009GL039706

Randel WJ et al (2009) An update of observed stratospheric temperature trend. J Geophys Res 114:D02107. doi:10.1029/2008JD010421

Ratnam MV, Kumar GK, Murthy BVK, Patra AK, Rao VVMJ, Rao SVB, Kumar KK, Ramkumar G (2008) Long-term variability of the low latitude mesospheric SAO and QBO and their relation with stratospheric QBO. Geophys Res Lett 35:L21809. doi:10.1029/2008GL035390

Remsberg EE (2007) A reanalysis for the seasonal and longer-period cycles and the trends in middle-atmosphere temperature from the halogen occultation experiment. J Geophys Res 112:D09118. doi:10.1029/2006JD007489

Remsberg EE (2009) Trends and solar cycle effects in temperature versus altitude from the halogen occultation experiment for the mesosphere and upper stratosphere. J Geophys Res 114:D12303. doi:10.1029/2009JD011897

Remsberg EE, Marshall BT, Garcia-Comas M, Krueger D, Lingenfelser GS, Martin-Torres J, Mlynczak MG, Russell JM III, Smith AK, Zhao Y, Brown C, Gordley LL, Lopez-Gonzalez MJ, Lopez-Puertas M, She CY, Taylor MJ, Thompson RE (2008) Assessment of the quality of the Version 1.07 temperature-versus-pressure profiles of the middle atmosphere from TIMED/SABER. J Geophys Res 113:D17101. doi:10.1029/2008JD010013

Ricciardulli L, Garcia RR (2000) The excitation of equatorial waves by deep convection in the NCAR community climate model (CCM3). J Atmos Sci 57:3461–3487

Richter JH, Sassi F, Garcia RR (2010) Towards a physically based gravity wave source parameterization in a general circulation model. J Atmos Sci 67:136–156

Richter JH, Matthes K, Calvo N, Gray LJ (2011) Influence of the quasi-biennial oscillation and El Niño-Southern Oscillation on the frequency of sudden stratospheric warmings. J Geophys Res 116:D20111. doi:10.1029/2011JD015757

Riggin DM, Lieberman RS, Vincent RA, Manson AH, Meek CE, Nakamura T, Tsuda T, Portnyagin YI (2004) The 2-day wave during the boreal summer of 1994. J Geophys Res 109:D08110. doi:10.1029/2003JD004493

Riggin DM, Liu HL, Lieberman RS, Roble RG, Russell JM III, Mertens CJ, Mlynczak MG, Pancheva D, Franke SJ, Murayama Y, Manson AH, Meek CE, Vincent RA (2006) Observations of the 5-day wave in the mesosphere and lower thermosphere. J Atmos Solar Terr Phys 68:323–339

Salby ML, Hartmann DL, Bailey P, Gille J (1984) Evidence for equatorial Kelvin modes in NIMBUS-7 LIMS. J Atmos Sci 41:220–235

Sassi F, Garcia R (1997) The role of equatorial waves forced by convection in the tropical semiannual oscillation. J Atmos Sci 54:1925–1942

Sato K, Watanabe S, Kawatani Y, Tomikawa Y, Miyazaki K, Takahashi M (2009) On the origins of mesospheric gravity waves. Geophys Res Lett 36:L19801. doi:10.1029/2009GL039908

Schmidt H, Brasseur GP, Charron M, Manzini E, Giorgetta MA, Diehl T, Fomichev VI, Kinnison D, Marsh D, Walters S (2006) The HAMMONIA chemistry climate model: sensitivity of the mesopause region to the 11-year solar cycle and CO_2 doubling. J Clim 19:3903–3931

She CY, Chen S, Williams BP, Hu Z, Krueger DA, Hagan ME (2002) Tides in the mesopause region over Fort Collins, Colorado (41°N, 105°W) based on lidar temperature observations covering full diurnal cycles. J Geophys Res 107:4350. doi:10.1029/2001JD001189

Shepherd TG (2000) The middle atmosphere. J Atmos Solar Terr Phys 62:1587–1601

Shine KP (1987) The middle atmosphere in the absence of dynamical heat fluxes. Q J R Meteorol Soc 113:603–633

Sinnhuber M (2012) Energetic particle precipitation and the chemistry of the mesosphere/lower thermosphere. Surv Geophys This issue

Simkhada DB, Snively JB, Taylor MJ, Franke SJ (2009) Analysis and modeling of ducted and evanescent gravity waves observed in the Hawaiian airglow. Ann Geophys 27:3213–3224

Siskind DE, Eckermann SD, McCormack JP, Alexander MJ, Bacmeister JT (2003) Hemispheric differences in the temperature of the summertime stratosphere and mesosphere. J Geophys Res 108:4051. doi:10.1029/2002JD002095

Siskind DE, Coy L, Espy P (2005) Observations of stratospheric warmings and mesospheric coolings by the TIMED SABER instrument. Geophys Res Lett 32:L09804. doi:10.1029/2005GL022399

Smith AK (1996) Longitudinal variations in mesospheric winds: evidence for gravity wave filtering by planetary waves. J Atmos Sci 53:1156–1173

Smith AK (1997) Stationary planetary waves in upper mesospheric winds. J Atmos Sci 54:2129–2145

Smith AK (2000) Structure of the terdiurnal tide at 95 km. Geophys Res Lett 27:177–180

Smith AK (2003) The origin of stationary planetary waves in the upper mesosphere. J Atmos Sci 60:3033–3041

Smith AK (2011) Interactions between the lower, middle and upper atmosphere. Space Sci Rev (Online First) doi:10.1007/s11214-011-9791-y

Smith AK, Ortland DA (2001) Modeling and analysis of the structure and generation of the terdiurnal tide. J Atmos Sci 58:3116–3134

Smith AK, Marsh DR, Szymczak AC (2003) Interaction of chemical heating and tides in the mesosphere. J Geophys Res 108:4164. doi:10.1029/2002JD002664

Smith AK, Pancheva DV, Mitchell NJ (2004) Observations and modeling of the 6-hour tide in the upper mesosphere. J Geophys Res 109:D10105. doi:10.1029/2003JD004421

Smith AK, Pancheva DV, Mitchell NJ, Marsh DR, Russell JM III, Mlynczak MG (2007) A link between variability of the semidiurnal tide and planetary waves in the opposite hemisphere. Geophys Res Lett 34:L07809. doi:10.1029/2006GL028929

Smith AK, Lopéz-Puertas M, García-Comas M, Tukiainen S (2009) SABER observations of mesospheric ozone during NH late winter 2002–2009. Geophys Res Lett 36:L23804. doi:10.1029/2009GL040942

Smith AK, Marsh DR, Mlynczak MG, Mast JC (2010a) Temporal variations of atomic oxygen in the upper mesosphere from SABER. J Geophys Res 115:D18309. doi:10.1029/2009JD013434

Smith AK, Garcia RR, Marsh DR, Kinnison DE, Richter JH (2010b) Simulations of the response of mesospheric circulation and temperature to the Antarctic ozone hole. Geophys Res Lett 37:L22803. doi:10.1029/2010GL045255

Smith AK, Garcia RR, Marsh DR, Richter JH (2011) WACCM simulations of the mean circulation and trace species transport in the winter mesosphere. J Geophys Res 116:D20115. doi:10.1029/2011JD016083

Smith S, Baumgardner J, Mendillo M (2009) Evidence of mesospheric gravity-waves generated by orographic forcing in the troposphere. Geophys Res Lett 36:L08807. doi:10.1029/2008GL036936

Snively JB, Pasko VP, Taylor MJ (2010) OH and OI airglow layer modulation by ducted short-period gravity waves: effects of trapping altitude. J Geophys Res 115:A11311. doi:10.1029/2009JA015236

Svoboda AA, Forbes JM, Miyahara S (2005) A space-based climatology of diurnal MLT tidal winds, temperatures and densities from UARS wind measurements. J Atmos Solar Terr Phys 67:1533–1543
Swinbank R, Ortland DA (2003) Compilation of wind data for the Upper Atmosphere Research Satellite (UARS) Reference Atmosphere Project. J Geophys Res 108:4615. doi:10.1029/2002JD003135
Takahashi H, Buriti R, Gobbi D, Batista P (2002) Equatorial planetary wave signatures observed in mesospheric airglow emissions. J Atmos Solar Terr Phys 64:1263–1272
Takahashi H, Wrasse CM, Fechine J, Pancheva D, Abdu MA, Batista IS, Lima LM, Batista PP, Clemesha BR, Schuch NJ, Shiokawa K, Gobbi D, Mlynczak MG, Russell JM (2007) Signatures of ultra fast Kelvin waves in the equatorial middle atmosphere and ionosphere. Geophys Res Lett 34:L11108. doi:10.1029/2007GL029612
Taori A, Dashora N, Raghunath K, Russell JM III, Mlynczak MG (2011) Simultaneous mesosphere–thermosphere–ionosphere parameter measurements over Gadanki (13.5°N, 79.2°E): First results. J Geophys Res 116:A07308. doi:10.1029/2010JA016154
Taylor MJ, Pendelton WR Jr, Clark S, Takahashi H, Gobbi D, Goldberg RA (1997) Image measurements of short-period gravity waves at equatorial latitudes. J Geophys Res 102:26,283–26,299
Taylor MJ, Pendelton WR Jr, Gardner CS, States RJ (1999) Comparison of terdiurnal tidal oscillations in mesospheric OH rotational temperature and Na lidar temperature measurements at mid-latitudes for fall/spring conditions. Earth Planets Space 51:877–885
Thompson D, Solomon S (2002) Interpretation of recent Southern Hemisphere climate change. Science 296:895–899. doi:10.1126/science.1069270
Vincent RA, Tsuda T, Karor S (1988) A comparative study of mesospheric solar tides observed at Adelaide and Kyoto. J Geophys Res 93:699–708
Vincent RA, Kovalam S, Fritts D, Isler JR (1998) Longterm MF radar observations of solar tides in the low-latitude mesosphere: interannual variability and comparisons with the GSWM. J Geophys Res 103:8667–8683
Wang DY, Ward WE, Shepherd GG, Wu DL (2000) Stationary planetary waves inferred from WINDII wind data taken within the altitudes 90–120 km during 1991–96. J Atmos Sci 57:1906–1918
Warner CD, McIntyre ME (2001) An ultra-simple spectral parameterization for non-orographic gravity waves. J Atmos Sci 58:1837–1857
Watanabe S, Miyahara S (2009) Quantification of the gravity wave forcing of the migrating diurnal tide in a gravity wave-resolving general circulation model. J Geophys Res 114:D07110. doi:10.1029/2008JD011218
Watanabe S, Kawatani Y, Tomikawa Y, Miyazaki K, Takahashi M, Sato K (2008) General aspects of a T213 L256 middle atmosphere general circulation model. J Geophys Res 113:D12110. doi:10.1029/2008JD010026
WMO (2010) Scientific assessment of ozone depletion: 2010. Global Ozone Research and Monitoring Project-Report No 52. Geneva, Switzerland
Wu Q, Ortland DA, Killeen TL, Roble RG, Hagan ME, Liu HL, Solomon SC, Xu J, Skinner WR, Niciejewski RJ (2008) Global distribution and interannual variations of mesospheric and lower thermospheric neutral wind diurnal tide: 1. Migrating tide. J Geophys Res 113:A05308. doi:10.1029/2007JA012542
Xiao C, Hu X, Tian J (2009) Global temperature stationary planetary waves extending from 20 to 120 km observed by TIMED/SABER. J Geophys Res 114:D17101. doi:10.1029/2008JD011349
Xu J, Liu H, Smith A, Roble R, Mertens C, Russell J III, Mlynczak M (2007a) Mesopause structure from thermosphere, ionosphere, mesosphere, energetics and dynamics (TIMED)/sounding of the atmosphere using broadband emission radiometry (SABER) observations. J Geophys Res 112:D09102. doi:10.1029/2006JD007711
Xu J, Smith AK, Yuan W, Liu H, Mlynczak MG, Russell JM III (2007b) Global structure and long-term variations of zonal mean temperature observed by TIMED/SABER. J Geophys Res 112:D24106. doi:10.1029/2007JD008546
Xu J, Smith AK, Liu H, Yuan W, Wu Q, Jiang G, Mlynczak MG, Russell J III (2009) Estimation of the equivalent Rayleigh friction in mesosphere/lower thermosphere region from the migrating diurnal tides observed by TIMED. J Geophys Res 114:D23103. doi:10.1029/2009JD012209
Xu J, Smith AK, Liu H, Yuan W, Wu Q, Jiang G, Mlynczak MG, Russell J III, Franke SJ (2009) Seasonal and quasi-biennial variations in the migrating diurnal tide observed by thermosphere, ionosphere, mesosphere, energetics and dynamics (TIMED). J Geophys Res 114:D13107. doi:10.1029/2008JD011298
Xu J, Smith AK, Jiang G, Yuan W (2010) Seasonal variation of the Hough modes of the diurnal component of ozone heating evaluated from Aura Microwave Limb Sounder observations. J Geophys Res 115:D10110. doi:10.1029/2009JD013179

Xu X, Manson AH, Meek CE, Chshyolkova T, Drummond JR, Hall CM, Riggin DM, Hibbins RE (2009) Vertical and interhemispheric links in the stratosphere-mesosphere as revealed by the day-to-day variability of Aura-MLS temperature data. Ann Geophys 27:3387–3409

Xu X, Manson AH, Meek CE, Chshyolkova T, Drummond JR, Riggin DM, Hall CM, Hibbins RE, Tsutsum M (2009) Asymmetry in the interhemispheric planetary wave-tide link between the two hemispheres. J Atmos Solar Terr Phys 71:1899–1903

Yamashita K, Miyahara S, Miyoshi Y, Kawano K, Ninomiya J (2002) Seasonal variation of non-migrating semidiurnal tide in the polar MLT region in a general circulation model. J Atmos Solar Terr Phys 64:1083–1094

Yamashita K, Liu H, Chu X (2010) Responses of mesosphere and lower thermosphere temperatures to gravity wave forcing during stratospheric sudden warming. Geophys Res Lett 37:L09803. doi:10.1029/2009GL042351

Younger PT, Mitchell NJ (2006) Waves with period near 3 days in the equatorial mesosphere and lower thermosphere over Ascension Island. J Atmos Solar Terr Phys 68:369–378

Younger PT, Pancheva D, Middleton HR, Mitchell NJ (2002) The 8h tide in the Arctic mesosphere and lower thermosphere. J Geophys Res 1420. doi:10.1029/2001JA005086

Yuan T, Schmidt H, She CY, Krueger DA, Reising S (2008) Seasonal variations of semidiurnal tidal perturbations in mesopause region temperature and zonal and meridional winds above Fort Collins, Colorado (40.6°N, 105.1°W). J Geophys Res 113:D20103. doi:10.1029/2007JD009687

von Zahn U, Hoffner J, Eska V, Alpers M (1996) The mesopause altitude: only two distinctive levels worldwide. Geophys Res Lett 23:3231–3234

Zhang SP, McLandress C, Shepherd GG (2007) Satellite observations of mean winds and tides in the lower thermosphere: 2. Wind Imaging Interferometer monthly winds for 1992 and 1993. J Geophys Res 112:D21105. doi:10.1029/2007JD008457

Zhang X, Forbes JM, Hagan ME, Russell III JM, Palo SE, Mertens CJ, Mlynczak MG (2006) Monthly tidal temperatures 20–120 km from TIMED/SABER. J Geophys Res 111. doi:10.1029/2005JA011504. EID A10S08